LA-UR-13-26886
Approved for public release; distribution is unlimited.

Title: Modelling and Simulation of Free Electron Lasers

Author(s): Freund, Henry P.

Intended for: DEPS Advanced High Power Lasers Conference, 2013-06-24 (Santa Fe, New Mexico, United States)

Issued: 2013-09-03

MODELING & SIMULATION OF FREE-ELECTRON LASERS

H.P. Freund
Los Alamos National Laboratory
Los Alamos, NM 87545

Minicourse Presented at the
Directed Energy Professional Society Advanced High Power Lasers Conference
June 2013
Santa Fe, New Mexico

OUTLINE

- One- and Three-Dimensional Formulations
- General Approach
    - Dynamical Equations
    - Steady-State vs Time-Dependent
    - Particle Loading Algorithm
    - Start-Up from Noise
    - Harmonics
    - Three-Dimensional Effects
    - Oscillators/Amplifiers
- Simulation-Generated Movie
- Code Benchmarking & Validation Examples

GENERAL FORMALISM

GENERAL FEL SCHEMATIC

In general, an FEL consists of an electron beam propagating through a wiggler.

The axial ponderomotive force is $(\mathbf{v}_w \times \mathbf{B}_R)_z$ acts to decelerate the beam. The energy lost by the beam in this way acts to amplify the electromagnetic wave.

FEL INTERACTION

- Electron beam undulates in wiggler and bunches at optical wavelength
- Optical radiation is amplified at the double-Doppler-shifted wavelength of the wiggler

Planar Wiggler

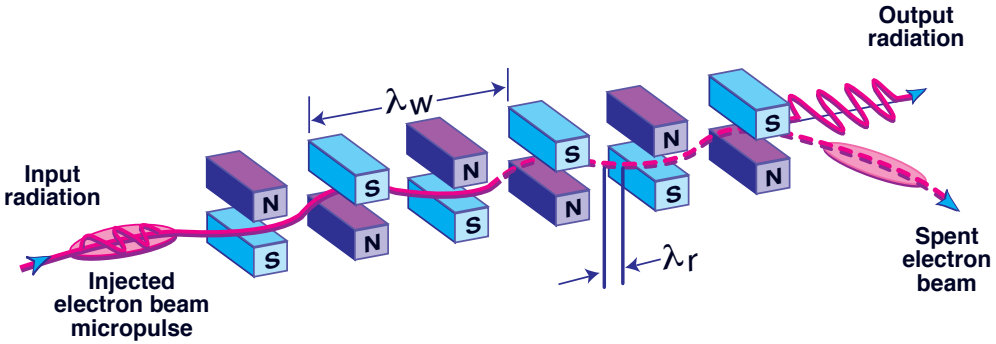

Helical Wiggler

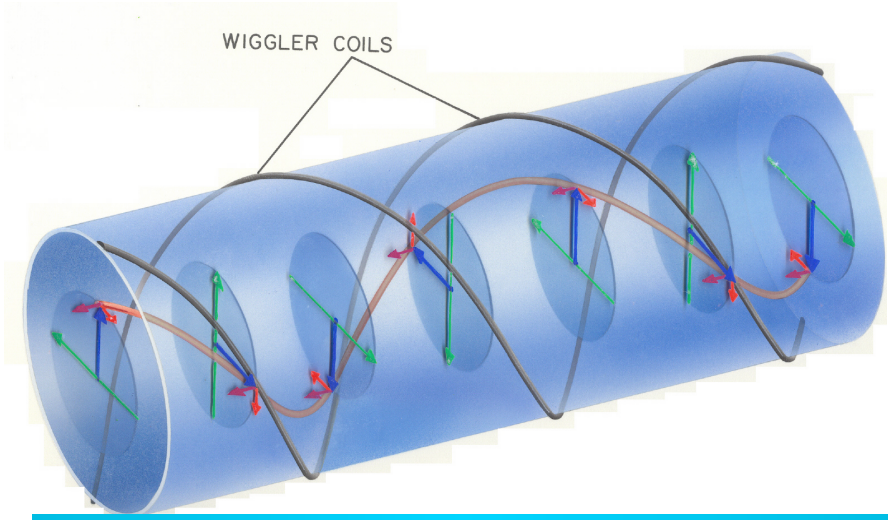

The effective wiggler strength is reduced to the rms wiggler field in a planar wiggler. Harmonic behavior is also different.

PRESENT STATE-OF-THE-ART IN FEL CODES

- **1-D Models:**
  - well-known - 20-30 year old formulations
- **3-D Models:**
  - Well-developed & **VALIDATED**
    - Amplifiers
      - MEDUSA, GINGER, GENESIS, TDA3D
    - Oscillators
      - MEDUSA, FELIX, NPS Codes
  - Scope for future development (?)
    - No major code development programs necessary
    - Physics-based modifications to present models
      - examples: harmonics in oscillators, real beam distributions
    - Engineering based application
      - **Start-to-End (S2E) simulation**

GENERAL SIMULATION FORMULATIONS

All FEL simulation codes include models for (1) the electromagnetic field, and (2) electron beam dynamics.

- The Electromagnetic Field
  - Slowly-Varying Envelope Approximation (SVEA) vs Particle-in-Cell (PiC) Simulation
  - Time-Domain vs Frequency Domain
  - Amplifier vs Oscillator vs SASE
  - Field Solver vs Modal Decomposition

- Particle Dynamics
  - Wiggler-Averaged vs Non-Wiggler-Averaged
  - Particle Loading
    - random vs deterministic
    - noise statistics

GENERAL INFORMATION ON MEDUSA

- Model Name: **MEDUSA**
  - Family of codes: ARACHNE, WIGGLIN, CHIFEL, MEDUSA, and MEDUSA1D
- Purpose: Simulation of FEL Amplifiers, Oscillators, and Harmonics
  - Entire wavelength spectrum/harmonics & sidebands
  - Multiple wiggler configurations
  - Additional focusing fields
  - Start-Up from Noise
  - Linked to OPC for oscillator simulations
    - Distortion modeling through OPC
- Principle Users & Applications
  - SAIC, LANL, Argonne Nat'l Lab
  - Amplifiers, Oscillators, SASE, OK/HGHG, Oscillators
- Development has been funded over the years by the ONR, JTO, DoE (ANL), SAIC, and myself

THE MEDUSA FAMILY OF FEL CODES

Property \ Code	ARACHNE	WIGGLIN	CHIFEL	MEDUSA
Creation	1985	1987	1995	1995
E & M Modes	Cylindrical Waveguide	Rectangular Waveguide	Coaxial Waveguide	Gaussian Optical
Wiggler Models	Helical	Planar	CHI	Planar or Helical
Polychrom-atic	Yes	No	No	Yes
Prebunched Beam	No	Yes	No	Yes
Additional B-Fields	No	No	No	Yes

IMPLEMENTATION/INTERFACE ISSUES

- **Programming Language:**
  - Fortran 90/95
    - Dynamic Memory Allocation
- **User Interface:**
  - Batch Mode/Command Line Execution
- **Operating Environment:**
  - Windows, Unix, Linux, Mac
- **Execution Times:**
  - Variable
    - From Seconds to Days (JLab FEL → 30-60 seconds/pass)
  - Parallelized: MPICH
    - Portable
    - Mac, PC, Beowulf, Supercomputers

TREATMENT OF THE ELECTROMAGNETIC FIELD

- All presently-used FEL codes employ the SVEA
  - When $\lambda_{res} << \lambda_w$ PiC models inappropriate.
- The envelope can vary in either space or space & time.
  - Fast oscillation removed via average over wave period
  - Variation slow compared to wavelength and wave period
- Time domain uses space & time variation
  - computationally intensive
- Frequency domain uses spatial variation
  - can include multiple wavelengths → oscillators & SASE
- Field Solver vs Modal Decomposition
  - Accuracy depends on either the grid spacing or the number of modes → affects run times

SIMPLIFIED 1-D SVEA FORMULATION

In a helical wiggler, the interaction is with a circularly polarized wave whose vector potential in the SVEA (amplitude varies in z only) representation is

$$\mathbf{A}_R = \delta A(z)\left[\hat{\boldsymbol{e}}_x \cos\,\varphi(z,t) - \hat{\boldsymbol{e}}_y \sin\,\varphi(z,t)\right]$$

$$\varphi(z,t) = \int_0^z dz' k(z') - \omega t \longrightarrow k = \frac{\partial \varphi}{\partial z}$$

Assumption: $\delta A(z)$ and $k(z)$ are nearly constant over a wavelength.

→ Neglect 2nd derivatives of the amplitude & phase

$$\left(\frac{\partial^2}{\partial z^2} - \frac{1}{c^2}\frac{\partial^2}{\partial t^2}\right)\mathbf{A}_R = -\frac{4\pi}{c} J_\perp(z,t)$$

$$\left(\frac{\omega^2}{c^2} - k^2\right)\delta A = -\frac{4\pi}{c}\left(J_x \cos\,\varphi - J_y \sin\,\varphi\right)$$

$$2k\frac{d}{dz}\delta A = \frac{4\pi}{c}\left(J_x \sin\,\varphi + J_y \cos\,\varphi\right)$$

HOW FAR CAN THE SVEA BE PUSHED?

For a variety of problems such as for pre-bunched beams, optical klystrons or high gain harmonic generation designs, the amplification can be faster than exponential; hence, it is useful to be able to treat problems where the field grows rapidly even when compared with the wiggler period. In these cases, the SVEA can be adapted to treat these problems.

- The 2nd order derivatives need not be neglected.
  - This adds equations and increases run times, but this is not prohibitive.
- There is no need to start with the 2nd order wave equation. Instead, the basic equations can be obtained from a Poynting's theorem approach which retains the 1st order nature of Maxwell's equations.

THE QUASI-STATIC APPROXIMATION

The source current for a mono-energetic can be represented as an integral over entry times t_0

$$\boldsymbol{J}(z,t) = -\,en_b\upsilon_{z0}\int_{-T}^{T} dt_0\sigma(t_0)\mathbf{v}(t,t_0)\frac{\delta\left[t-\tau(z,t_0)\right]}{\upsilon_z(t,t_0)}$$

$$\tau(z,t_0) = t_0 + \int_0^z \frac{dz'}{\upsilon_z(z',t_0)}$$

Quasi-Static Assumption: particles entering the interaction region at intervals of the wave period execute the same trajectories

$$\rightarrow \mathbf{v}(t+2\pi N/\omega, t_0+2\pi N/\omega) = \mathbf{v}(t,t_0)$$

$$\int_0^{2\pi/\omega} dt\int_{-T}^{T} dt_0 G(z,t,t_0)\delta\left[t-\tau(z,t_0)\right] = \int_0^{2\pi/\omega} dt_0 G\left[z,\tau(z,t_0),t_0\right]$$

Average is over "initial" state

TIME-AVERAGED MAXWELL EQUATIONS

Averaging Maxwell's equations over a wave period, then yields

$$\left(\frac{\omega^2}{c^2} - k^2\right)\delta a = \frac{\omega_b^2}{c^2}\beta_{z0}\left\langle \frac{v_1 \cos\psi - v_2 \sin\psi}{|v_z|}\right\rangle$$

$$2k\frac{d}{dz}\delta a = -\frac{\omega_b^2}{c^2}\beta_{z0}\left\langle \frac{v_1 \sin\psi - v_2 \cos\psi}{|v_z|}\right\rangle$$

$v_1 = v_x \cos k_w z + v_y \sin k_w z$

$v_2 = -v_x \sin k_w z + v_y \cos k_w z$

→ Frame rotating with a helical wiggler

$\langle(\cdots)\rangle \equiv \frac{1}{2\pi}\int_0^{2\pi} d\psi_0(\cdots)$ → N.B.: this assumes a monoenergetic initial state

$\psi = \psi_0 + \int_0^z dz'\left(k + k_w - \frac{\omega}{v_z}\right)$ → Ponderomeotive Phase

PHYSICAL MEANING OF THE SVEA

- This fast time scale has been removed and we treat the co-propagation of a "beamlet" with the wave
  - Quasi-static assumption implies a CW beam
    - $\lambda << cT$ → electron bunch is many wavelengths long
    - "Steady-state" interaction – each bunch interacts in an identical manner
  - The field at some point z is the average value determined by the interaction of those particles that pass that point in one wave period

TREATMENT OF PARTICLE DYNAMICS

- Wiggler-Averaged Formulation (also called KMR Model)
  - Originally developed because early simulations were not typically run on supercomputers.
  - Model integrates 2 equations: ponderomotive phase and energy.
    - transverse motion is approximate.
    - wiggle motion is included through the pendulum equation.
      - large integration steps ($> \lambda_w$).

- Non-Wiggler-Average Formulation
  - First Principles Integration of the Lorentz force equations.
  - Longer run times than KMR models.
  - Harmonic interactions implicitly included in particle dynamics.
  - Ease of handling complex magnetic fields (wigglers, chicanes, optical klystrons, quadrupoles, etc.).
    - same integration engine.

1-D PARTICLE DYNAMICS

For each macro-particle, we integrate 4 equations:

$$\frac{d\psi}{dt} = k + k_w - \frac{\omega}{v_z}$$

The ponderomotive phase represents a Lagrangian time coordinate that substitutes for integration over dz/dt

$$\frac{d}{dt}\,\mathbf{p} = -\,e\delta\mathbf{E} - \frac{e}{c}\,\mathbf{v}\times\left(\mathbf{B}_{ext} + \delta\mathbf{B}\right)$$

Full relativistic dynamics for three momentum components using the magnetostatic (wiggler, solenoid, etc.) and radiation fields

PARTICLE LOADING ALGORITHM

• Particle loading done differently in **MEDUSA** than in most other FEL codes, and uses a deterministic algorithm

• Amplification is governed by

$$2k\frac{d}{dz}\delta a = -\frac{\omega_b^2}{c^2}\beta_{z0}\left\langle \frac{\upsilon_1 \sin\psi - \upsilon_2 \cos\psi}{|\upsilon_z|}\right\rangle$$

$$\langle \sin\psi\rangle = \frac{1}{2\pi}\int_0^{2\pi} d\psi_0 F(\psi_0)\sin\psi$$

Initial phase distribution

discretize integration →

$$= \frac{1}{2\pi}\sum_n w_i F(\psi_i)\sin\psi_i$$

→ Gaussian Quadrature

An 8-point Gaussian integration for a uniform phase will yield a null phase average to within machine accuracy

→ QUIET START is implicit in the algorithm

1-D MODEL VALIDATION

1-D model validation performed by comparison with linear theory for helical wiggler with axial solenoidal field

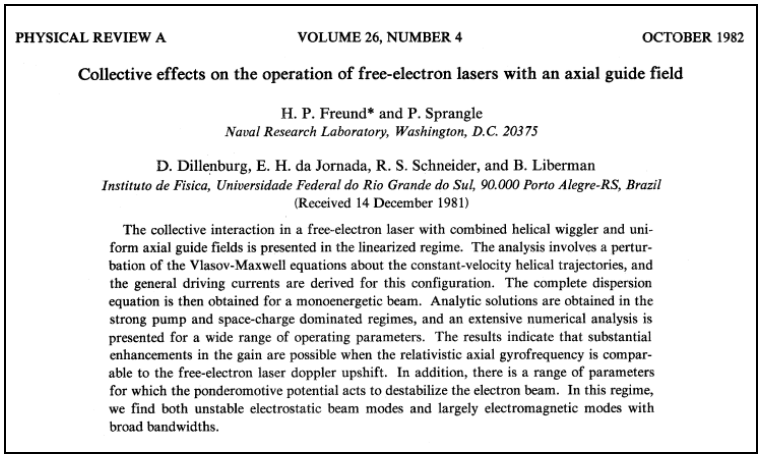

PHYSICAL REVIEW A VOLUME 26, NUMBER 4 OCTOBER 1982

Collective effects on the operation of free-electron lasers with an axial guide field

H. P. Freund* and P. Sprangle
Naval Research Laboratory, Washington, D.C. 20375

D. Dillenburg, E. H. da Jornada, R. S. Schneider, and B. Liberman
Instituto de Fisica, Universidade Federal do Rio Grande do Sul, 90.000 Porto Alegre-RS, Brazil
(Received 14 December 1981)

The collective interaction in a free-electron laser with combined helical wiggler and uniform axial guide fields is presented in the linearized regime. The analysis involves a perturbation of the Vlasov-Maxwell equations about the constant-velocity helical trajectories, and the general driving currents are derived for this configuration. The complete dispersion equation is then obtained for a monoenergetic beam. Analytic solutions are obtained in the strong pump and space-charge dominated regimes, and an extensive numerical analysis is presented for a wide range of operating parameters. The results indicate that substantial enhancements in the gain are possible when the relativistic axial gyrofrequency is comparable to the free-electron laser doppler upshift. In addition, there is a range of parameters for which the ponderomotive potential acts to destabilize the electron beam. In this regime, we find both unstable electrostatic beam modes and largely electromagnetic modes with broad bandwidths.

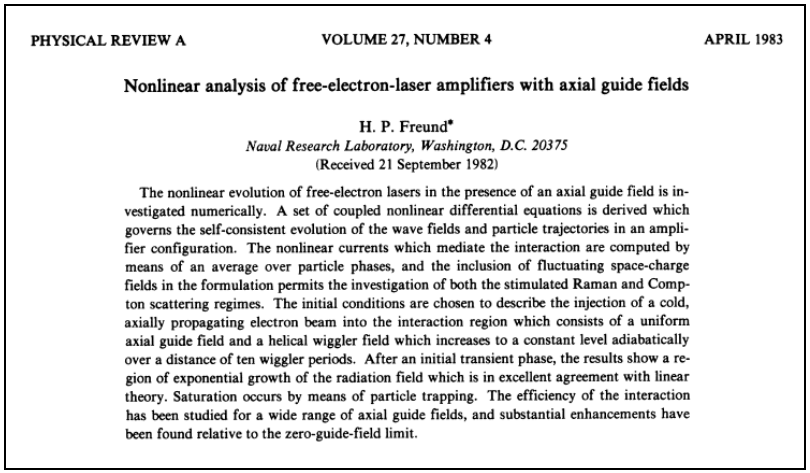

PHYSICAL REVIEW A VOLUME 27, NUMBER 4 APRIL 1983

Nonlinear analysis of free-electron-laser amplifiers with axial guide fields

H. P. Freund*
Naval Research Laboratory, Washington, D.C. 20375
(Received 21 September 1982)

The nonlinear evolution of free-electron lasers in the presence of an axial guide field is investigated numerically. A set of coupled nonlinear differential equations is derived which governs the self-consistent evolution of the wave fields and particle trajectories in an amplifier configuration. The nonlinear currents which mediate the interaction are computed by means of an average over particle phases, and the inclusion of fluctuating space-charge fields in the formulation permits the investigation of both the stimulated Raman and Compton scattering regimes. The initial conditions are chosen to describe the injection of a cold, axially propagating electron beam into the interaction region which consists of a uniform axial guide field and a helical wiggler field which increases to a constant level adiabatically over a distance of ten wiggler periods. After an initial transient phase, the results show a region of exponential growth of the radiation field which is in excellent agreement with linear theory. Saturation occurs by means of particle trapping. The efficiency of the interaction has been studied for a wide range of axial guide fields, and substantial enhancements have been found relative to the zero-guide-field limit.

$$\delta k\left(\delta k + 2\kappa\right)\left(\delta k - \Delta k\right) \cong -\frac{\upsilon_w^2}{2\upsilon_z^2}\frac{\omega_b^2 k_w}{\gamma_0\gamma_z^2 c^2}\Phi$$

$$\delta k = k - \frac{\omega}{\upsilon_z} - \kappa$$

$$\kappa = \frac{\omega_b}{\gamma_0^{1/2}\gamma_z c}\Phi^{1/2} \longrightarrow \text{Space-Charge Parameter}$$

$$\Delta k = \frac{\sqrt{\omega^2 - \omega_b^2/\gamma_0}}{c} + k_w - \frac{\omega}{\upsilon_z} - \kappa \longrightarrow \text{Detuning Parameter}$$

NON-WIGGLER-AVERAGED FORMULATION

While Maxwell's equations are averaged over a wave period, there is no need to average the Lorentz force equations. A first principles treatment of particle dynamics has the following advantages:

- All harmonic/sideband behavior is implicitly preserved.
- Complex magnetic fields (wigglers, dipoles, chicanes, quadrupoles, optical klystrons, etc.) can be added with minimal effort.

The first principles approach introduces no further assumptions or approximations into the formulation. Beowulf clusters can be expected to further facilitate this approach by reducing run times.

1-D ORBITS: HELICAL WIGGLER & SOLENOID

The solenoid acts to increase the transverse velocity and can increase the coupling coefficient

$$\frac{\upsilon_z^2}{c^2}\left(1+\frac{\Omega_w^2}{\left(\Omega_0-k_w\upsilon_z\right)^2}\right)\cong 1-\frac{1}{\gamma_0^2}$$

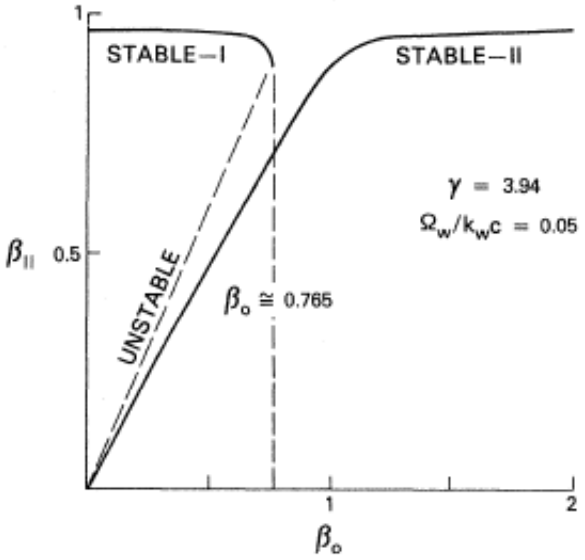

Negative mass instability is possible for strong solenoidal fields in the Group II regime

$$\frac{d\upsilon_z}{d\gamma_0}\propto \Phi$$

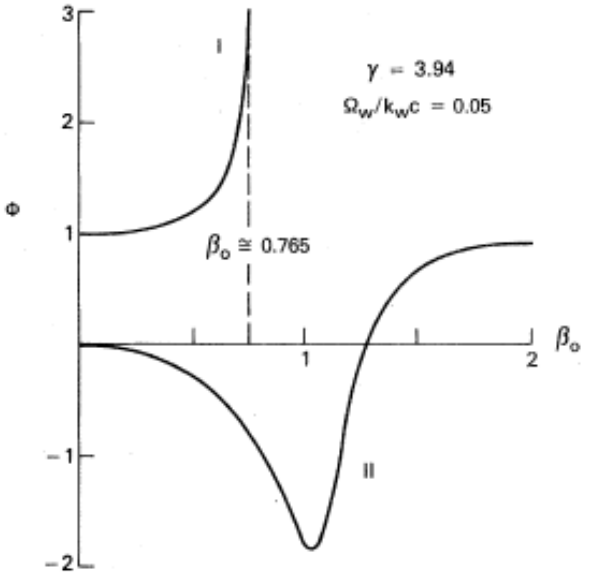

DISTRIBUTION A

1-D GAIN COMPARISONS

Simulation shows uniform growth rate yielding exponential gain until saturation

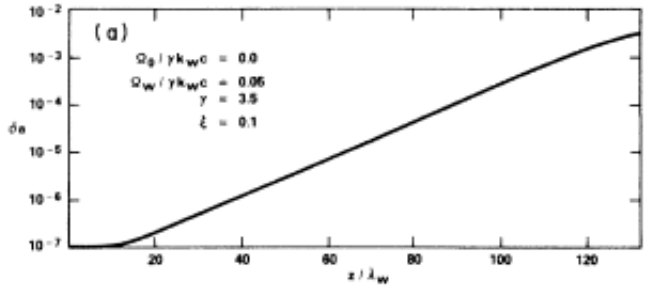

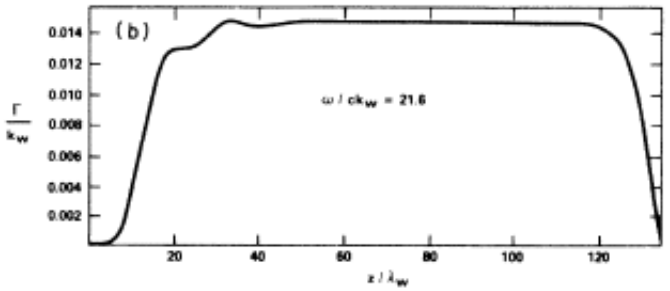

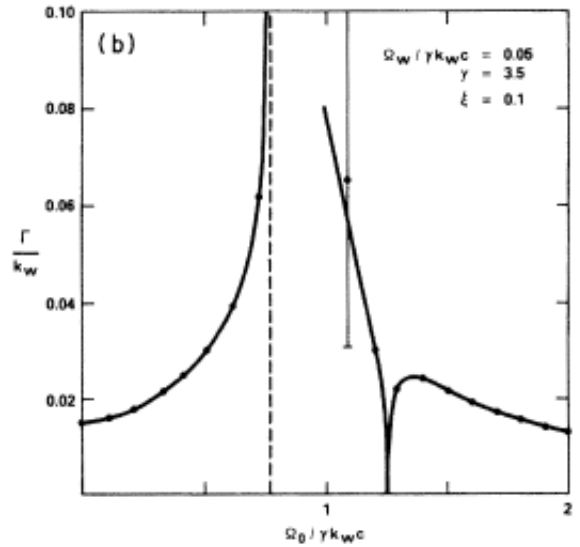

Comparison with the linear dispersion equation shows good agreement with the simulation. The "error bars" for one point are due to a mismatched beam injection leading to fluctuations about a mean growth rate

1-D COMPARISON OF SATURATION EFFICIENCY

The parameters correspond to the Raman regime where space charge forces dominate over the ponderomotive potential. The saturation efficiency is given by

$$\eta = \frac{\sqrt{1+K^2}}{\gamma_0}\,\frac{\omega_b}{\gamma_0^{1/2}k_w c} \approx 4\%$$

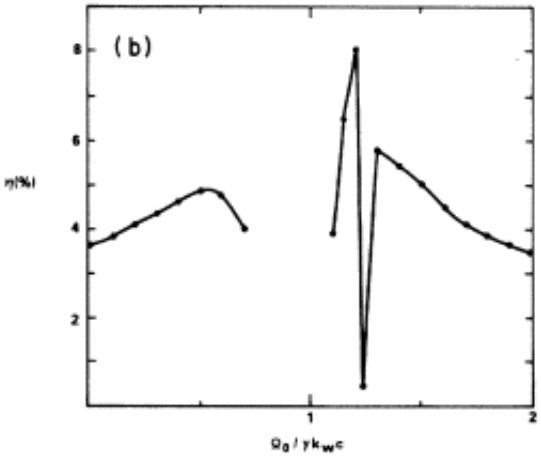

This is in good agreement with the simulation for $B_0 = 0$.

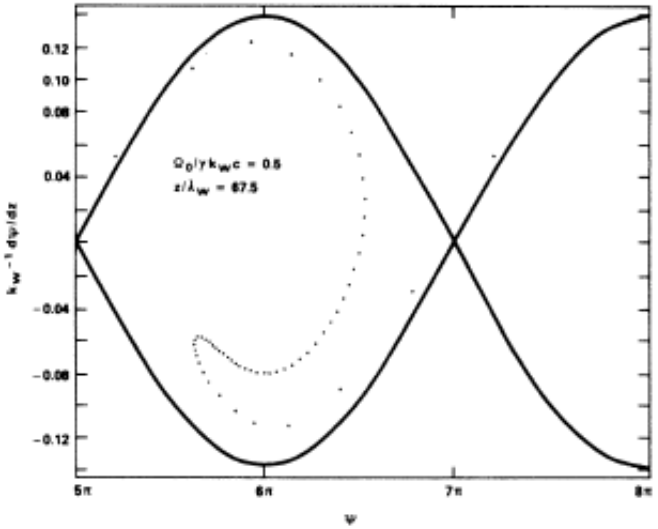

The phase space at saturation shows the expected trapped particle distribution. Note that not all electrons are trapped. **The number of simulation particles must be large enough to predict this trapping fraction**.

POLYCHROMATIC GENERALIZATION

We can include multiple wavelengths by explicitly including a "Fourier Spectrum" of regularly-spaced frequencies in the field representation

$$\mathbf{A}_R = \sum_n \delta A_n(z)\left[\hat{\boldsymbol{e}}_x \cos\,\varphi_n(z,t) - \hat{\boldsymbol{e}}_y \sin\,\varphi_n(z,t)\right]$$

$$\varphi_n(z,t) = \int_0^z dz' k_n(z') - n\Delta\omega t$$

Average Maxwell's equations over $\Delta\tau = 2\pi/\Delta\omega$ "projects out" each frequency component.

- The "beamlet" now stretches over a longer interval, requiring more particles and longer run times.
  - **Quasi-static assumption can be relaxed to include details of pulse shape.**
- Allows us to treat harmonics and sidebands.
- Allows us to treat time-dependent behavior.
  - Temporal behavior using an inverse FFT.

TIME-DEPENDENCE/SLIPPAGE

- These equations for the (z,t) SVEA are solved by breaking the pulse into "slices" for both the beam and radiation.
  - Each slice is treated as in the steady-state, and the slippage is applied to the radiation slices to advance the field.
  - Can apply this to harmonics also.
- **This is equivalent to the explicit harmonic expansion for polychromatic fields.**

- At resonance, the radiation slips ahead of the electron by one wavelength/wiggler period.
  - Can result in pulse distortions and reduced gain.
  - Must include"blank" radiation slices.

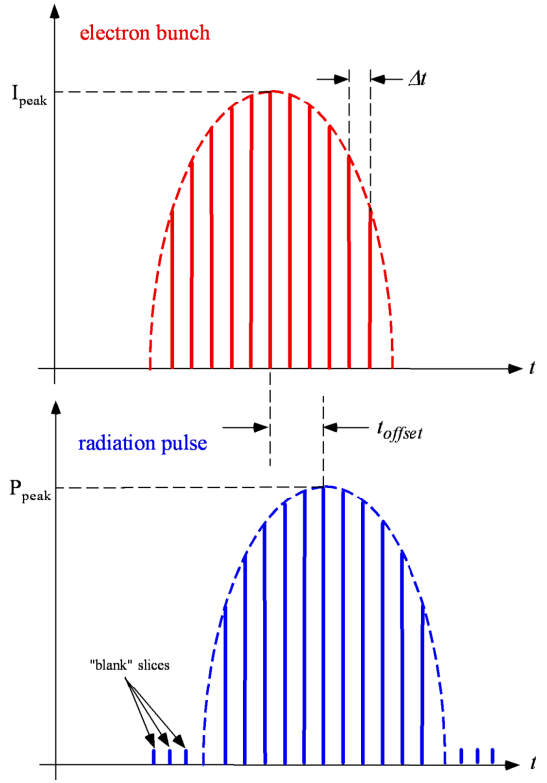

TIME-DEPENDENT MAXWELL'S EQUATIONS

In treating time-dependence, we express the vector potential as

$$\delta\mathbf{A}(z,t) = \sum_{h=1}^{\infty} \delta A_h^{(1)}\left[\hat{\mathbf{e}}_x \cos\varphi_h - \hat{\mathbf{e}}_y \sin\varphi_h\right] - \sum_{h=1}^{\infty} \delta A_h^{(2)}\left[\hat{\mathbf{e}}_x \sin\varphi_h + \hat{\mathbf{e}}_y \cos\varphi_h\right]$$

So the dynamical equations for each harmonic field component are

$$\left(\frac{\partial}{\partial z} + \frac{1}{c}\frac{\partial}{\partial t}\right)\begin{pmatrix} \delta a_h^{(1)} \\ \delta a_h^{(2)} \end{pmatrix} = -\frac{\omega_b^2}{2h\omega c}\begin{pmatrix} \left\langle \dfrac{v_x \sin\varphi_h + v_y \cos\varphi_h}{|v_z|} \right\rangle \\ \left\langle \dfrac{v_x \cos\varphi_h - v_y \sin\varphi_h}{|v_z|} \right\rangle \end{pmatrix}$$

In practice, we integrate $z \rightarrow z + \Delta z$ and then apply the slippage (*i.e.*, the time derivative) using the forward time-derivative to ensure that information does not propagate backward in z.

TIME DEPENDENCE vs POLYCHROMATIC

- Equivalent Approaches
  - Explicit Fourier Spectrum in the Polychromatic Extension is Formally Equivalent to the Multi-Slice Time-Dependent Formulation
- Polychromatic Approach
  - Harmonics
  - Sidebands ($\Delta\omega << \omega_{res}$)
- Time-Dependent Approach
  - Sidebands
- Combination
  - Time-Dependence & Polychromatic allows harmonics & time-dependence

SIMULATING SHOT NOISE

- Most seeded simulations assume that $\langle \exp(i\psi) \rangle = 0$ and will not start unless it is seeded.
  - Real beams contain shot noise that satisfies Poisson statistics where $\langle \exp(i\psi) \rangle = 1/\sqrt{N}$, where N = number of correlated electrons.
- Need to develop an algorithm that introduces the corresponding "jitter" into the initial phase distribution.
- Algorithm developed on ONR-sponsored visit to ENEA-Frascati.
- Choose jitter magnitude $\delta\psi_1 = 1/\sqrt{N}$ and $h\delta\psi_h = \delta\psi_1$, then select jitter ϕ using a random number generator

$$\psi'_{0j} = \psi_{0j} + \sum_{h=1}^{h_{max}} \delta\psi_h \sin\left[h\left(\psi_{0j} - \phi\right)\right]$$

- Works for fundamental & harmonics
- Good agreement for MEDUSA1D & PERSEO (in-house at Frascati)

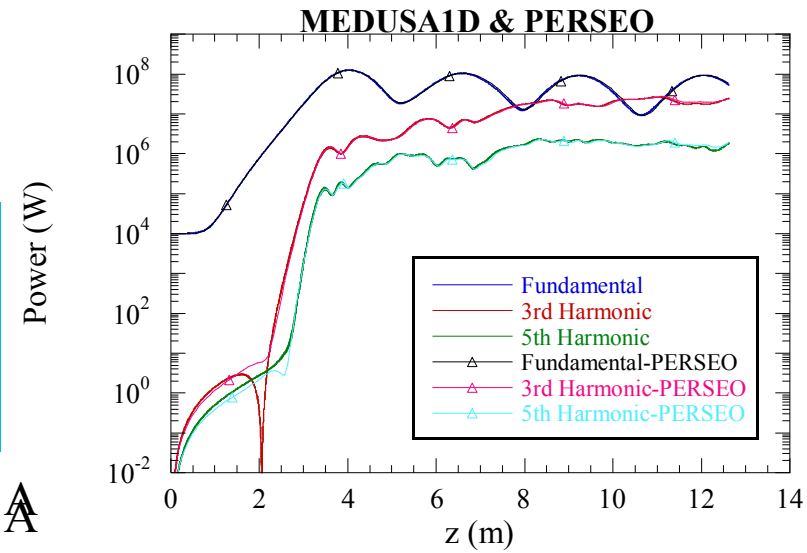

DISTRIBUTION A

THREE-DIMENSIONAL EEFECTS: BEAM QUALITY

• The FEL interaction depends on the axial bunching of the beam, and is sensitive to the axial energy spread. This can arise from various causes:

• **Energy Spread:** may be correlated or uncorrelated

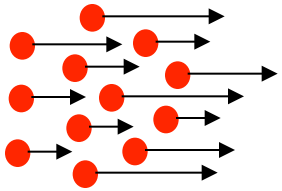

• **Emittance:** phase space area ($R_b \Delta\theta$) → angular spread

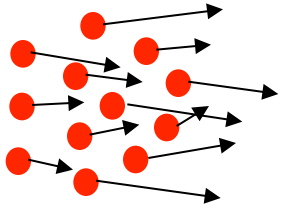

• **Wiggler Gradients:** transverse shear in wiggler → velocity shear

$$\frac{\Delta\gamma_z}{\gamma_b} = \frac{\gamma_z}{\gamma_b}\frac{\Delta\gamma_{th}}{\gamma_b} + \frac{1}{2}\left(\frac{\varepsilon_n}{R_b}\right)^2\left(\frac{\gamma_z}{\gamma_b}\right)^3 + \left(\frac{k_w R_b}{2}\frac{K}{\gamma_b}\right)^2$$

THREE-DIMENSIONAL EFFECTS:OPTICAL GUIDING

• The electron beam acts like a optical fiber that can confine the bulk of the radiation to within the electron beam.

• The light is optically guided by two related mechanisms
  • Gain Guiding: Rays don't grow away from the e-beam
  • Refractive Guiding: Wavenumber shift → e-beam acts like an optical fiber

Leads to an extended interaction length where the coupling is high.

LEUTL at Argonne Nat'l Lab →

$L_G \approx 0.5$ m

$z_R \approx 1.5$ m

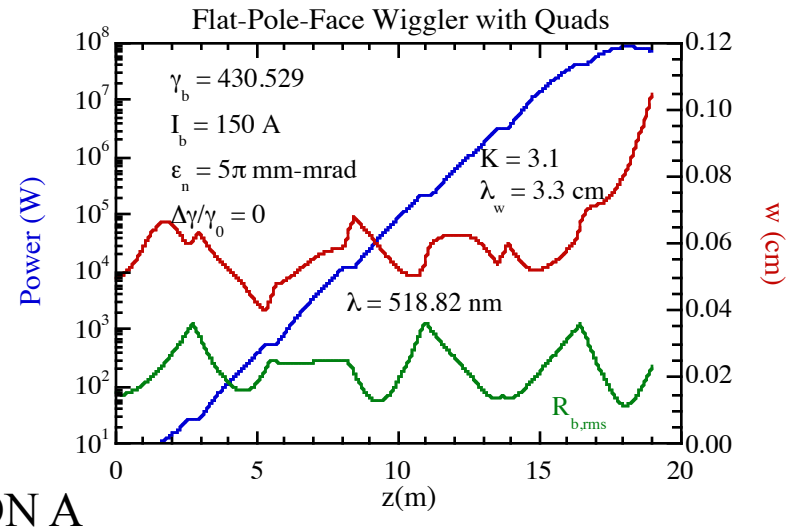

FINITE PULSE LENGTH EFFECTS

SLIPPAGE: Describes the tendency of the e-beam to lag behind the light pulse. Unimportant when $s < v_b \tau_p$.

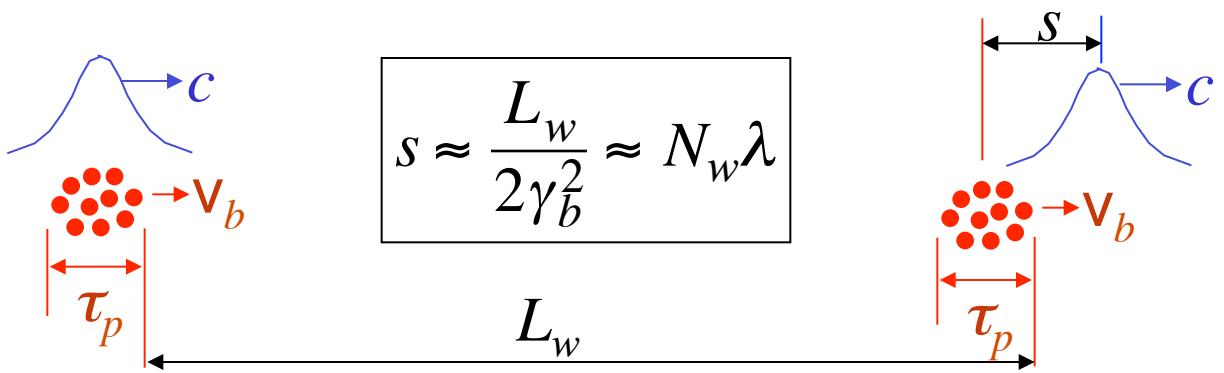

$$s \approx \frac{L_w}{2\gamma_b^2} \approx N_w \lambda$$

LETHARGY: describes the distortion of the pulse shape due to slippage. Trailing edge of pulse undergoes more growth than the leading edge.

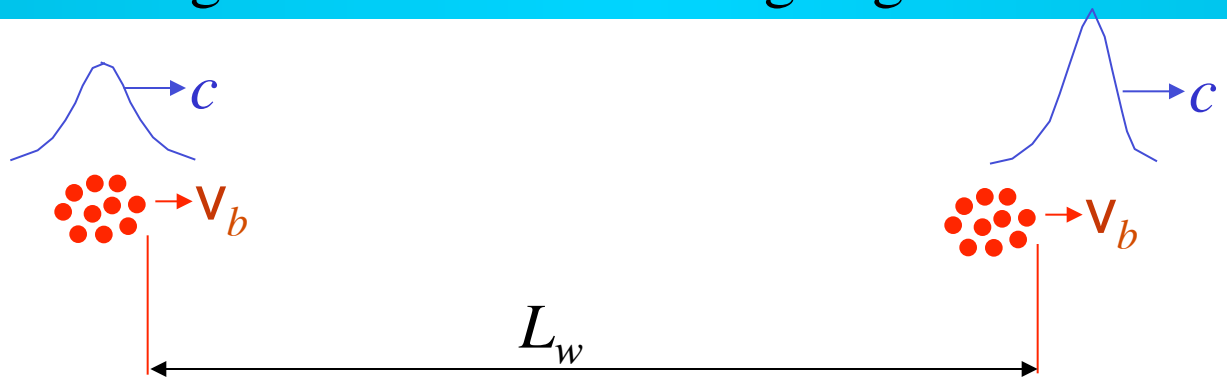

THREE-DIMENSIONAL GENERALIZATION

The 1-D formulation can be readily generalized to 3-D by including a polarization function that varies in (x,y) or (r,θ) in addition to the sinusoidal variation is (z,t).

$$\mathbf{A}_R = \frac{1}{2}\,\delta A(z)\,\boldsymbol{e}_\perp(x,y)e^{i\varphi(z,t)} + c.c.$$

polarization function

The polarization function can be derived from:

- Field solver – Accuracy depends on fineness of the grid
  - boundary value problem
- Modal decomposition – Accuracy depends on the number of modes
  - Waveguide modes (cylindrical, rectangular, etc.)
  - Gaussian optical modes (Hermite, Laguerre)

THREE-DIMENSIONAL MODAL EXPANSION

We use a Slowly-Varying Envelope Approximation in z and t along with a superposition of Gauss-Hermite modes. This permits the inclusion of **explicit time-dependence**

$$\delta\mathbf{A}(\mathbf{x},t) = \hat{\mathbf{e}}_x \sum_{l,n,h} e_{l,n,h}(x,y)\left[\delta A^{(1)}_{l,n,h}(z,t)\cos\varphi_h + \delta A^{(2)}_{l,n,h}(z,t)\sin\varphi_h\right]$$

$$e_{l,n,h}(x,y) = e^{-r^2/w_h^2(z,t)}\, H_l\!\left(\frac{\sqrt{2}x}{w_h(z,t)}\right) H_n\!\left(\frac{\sqrt{2}y}{w_h(z,t)}\right)$$

$$\varphi_h = h\left(k_0 z - \omega_0 t\right) + \alpha_h(z,t)\,\frac{r^2}{w_h^2(z,t)}$$

Spot Size

Curvature

A Source-Dependent Expansion [Sprangle *et al.*, Phys. Rev. A **36**, 202 (1987)] is used to track the evolution of the slowly-varying amplitudes, spot size, and curvature

THREE-DIMENSIONAL FIELD EQUATIONS

$$\left(\frac{\partial}{\partial z}+\frac{1}{c}\frac{\partial}{\partial t}+\frac{w_h'}{w_h}\right)\begin{pmatrix}\delta a_{l,n,h}^{(1)}\\ \delta a_{l,n,h}^{(2)}\end{pmatrix}+K_{l,n,h}\begin{pmatrix}\delta a_{l,n,h}^{(2)}\\ -\delta a_{l,n,h}^{(1)}\end{pmatrix}=\begin{pmatrix}s_{l,n,h}^{(1)}\\ s_{l,n,h}^{(2)}\end{pmatrix}$$

$$w_h'=\left(\frac{\partial}{\partial z}+\frac{1}{c}\frac{\partial}{\partial t}\right)w_h=\frac{2\alpha_h}{hk_0w_h}-w_hY_h$$

$$\alpha_h'=\left(\frac{\partial}{\partial z}+\frac{1}{c}\frac{\partial}{\partial t}\right)\alpha_h=\frac{2\left(1+\alpha_h^2\right)}{hk_0w_h^2}-2\left(X_h+\alpha_hY_h\right)$$

$$K_{l,n,h}=\left(l+n+1\right)\left(\alpha_h\frac{w_h'}{w_h}-\frac{\alpha_h'}{2}-\frac{1+\alpha_h^2}{hk_0w_h^2}\right)$$

$$\begin{pmatrix}s_{l,n,h}^{(1)}\\ s_{l,n,h}^{(2)}\end{pmatrix}=\frac{2\omega_b^2}{hk_0c^2}\frac{1}{2^{l+n}l!n!w_h^2}\left\langle\frac{v_x}{|v_z|}e_{l,n,h}\begin{pmatrix}\cos\varphi_h\\ -\sin\varphi_h\end{pmatrix}\right\rangle$$

$$X_h=2\frac{\left(s_{2,0,h}^{(1)}+s_{0,2,h}^{(1)}\right)\delta a_{0,0,h}^{(2)}-\left(s_{2,0,h}^{(2)}+s_{0,2,h}^{(2)}\right)\delta a_{0,0,h}^{(1)}}{\delta a_{0,0,h}{}^2}$$

$$Y_h=-2\frac{\left(s_{2,0,h}^{(1)}+s_{0,2,h}^{(1)}\right)\delta a_{0,0,h}^{(1)}+\left(s_{2,0,h}^{(2)}+s_{0,2,h}^{(2)}\right)\delta a_{0,0,h}^{(2)}}{\delta a_{0,0,h}{}^2}$$

THREE-DIMENSIONAL AVERAGING OPERATOR

We use a Gaussian distribution function

$$\left\langle (\cdots) \right\rangle \equiv \int_0^{2\pi} \frac{d\psi_0}{2\pi} \int_0^{\infty} d\gamma_0 \, \frac{\exp\left[-\left(\gamma - \bar{\gamma}_0\right)^2 / 2\Delta\gamma^2\right]}{\sqrt{\pi/2}\,\Delta\gamma\left[1 + \mathrm{erf}\left(\bar{\gamma}_0 / \sqrt{2}\,\Delta\gamma\right)\right]}$$

$$\times \int\int\int\int dx_0 dy_0 dp_{x0} dp_{y0} \frac{\exp\left(-r_0^2/2\sigma_r^2 - p_{\perp 0}^2/2\sigma_p^2\right)}{(2\pi)^2 \sigma_r^2 \sigma_p^2} \, (\cdots)$$

Macro-particles are loaded using the Gaussian Quadrature algorithm

- Efficient
- Implicit quiet start

THREE-DIMENSIONAL PARTICLE DYNAMICS

We now have 6 equations per particle, as well as the field equations

$$\frac{dx}{dt} = v_x$$

$$\frac{dy}{dt} = v_y$$

$$\frac{d\psi}{dt} = k + k_w - \frac{\omega}{v_z}$$

$$\frac{d}{dt}\,\mathbf{p} = -\,e\delta\mathbf{E} - \frac{e}{c}\,\mathbf{v} \times \left(\mathbf{B}_{ext} + \delta\mathbf{B}\right)$$

NUMERICAL ALGORITHM

- Integration of the dynamical equations using a 4^{th}-order Runge-Kutta algorithm
  - Permits variable step size
    - Important in treating multiple wiggler segments, drift spaces, magnetic dipoles and quadrupoles
  - The number of equations is

$$N = [6N_{particles} + 2N_{modes} + 2\,N_{harmonics}]N_{slices}$$

  - Parallelizable on the number of slices

PARALLELIZATION - MEDUSA

- Parallelization important for treating "large" simulations since single CPU runs are too long
  - SASE/start-up from noise/many "slices"
  - Time-dependence/many "slices"
- Message Passing Interface (MPI) is a standard and transportable protocol
  - Works best for independent tasks
  - Communication between slices required to treat slippage will limit advantage
  - Computer architecture will also affect run times
    - Beowulf cluster versus shared memory systems
    - Type of interconnect (ethernet vs miranet)

- Example: Beowulf cluster at SAIC
  - 3.2 GHz Xeons/Gigabit ethernet
- "Ideal" case would show a slope of unity
  - Indicates efficient use of cluster
- The curve hasn't begun to roll over indicating the further gains would be possible using still more cpu's

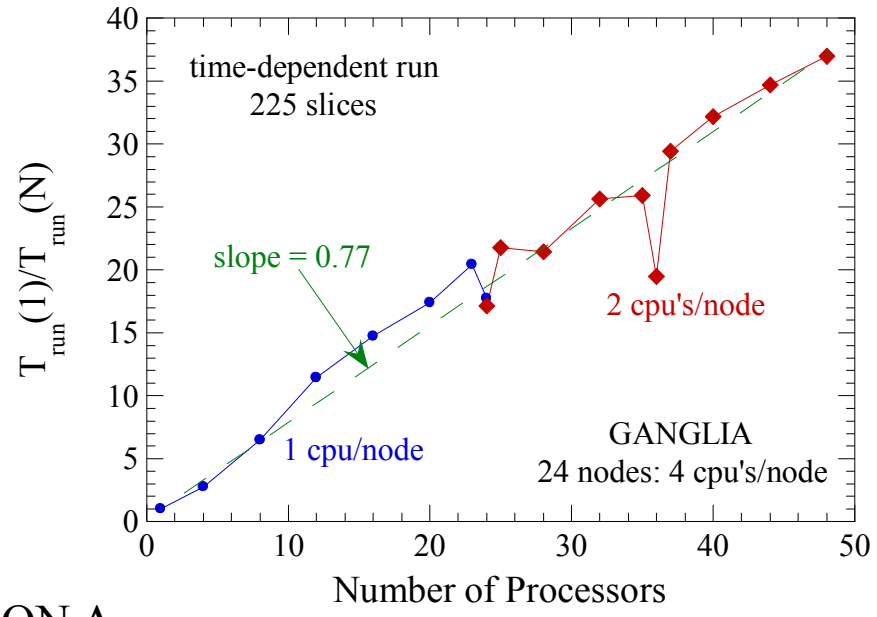

OSCILLATORS: MEDUSA/OPC

- OPC is an optics propagation code that propagates the field using either a Spectral Method or a Modified Fresnel Diffraction Integral both of which are solved using FFTs.
- MEDUSA hands off the field at the exit from the wiggler, and OPC propagates the field to the downstream mirror, the upstream mirror, and back to the wiggler entrance.

- OPC treats mirror distortion (Zernike polynomials), hole or transmissive out-coupling, dispersive optical elements in the resonator, different resonator designs, harmonic propagation, and more.
- MEDUSA & OPC both use MPI.
- MEDUSA/OPC interface is written in PERL.
  - We wrote translators for MEDUSA ←→ OPC.

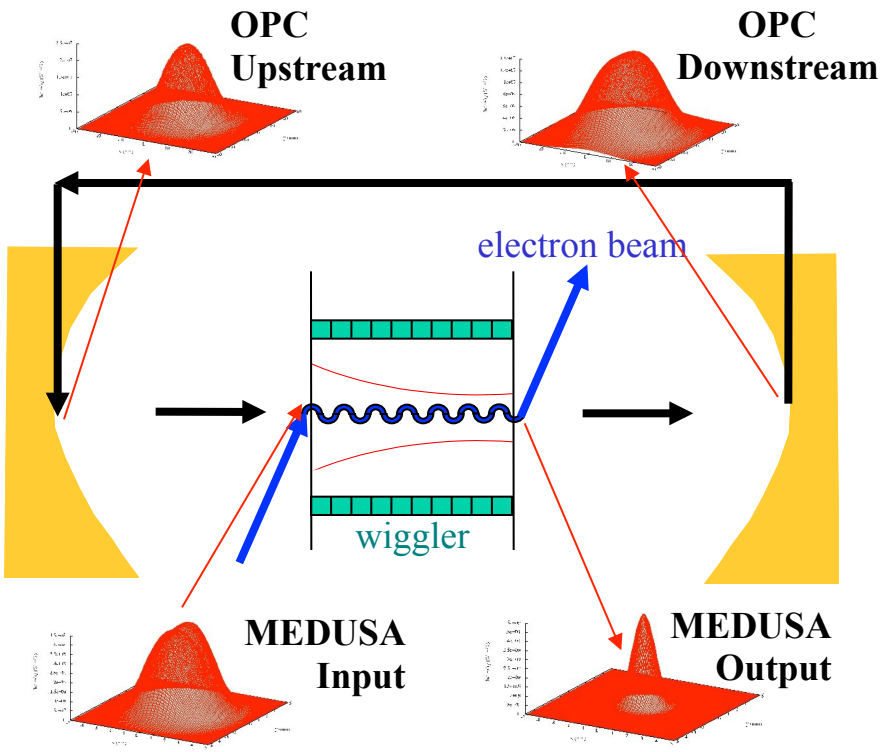

HARMONIC GENERATION

- FELs implicitly generate more harmonic power than conventional lasers
  - Similar to difference between solid state & vacuum tube audio amplifiers
  - Due to harmonic bunching of the electron beam

- Important in both amplifiers & oscillators
  - Degradation of mirror coatings – especially for UV harmonics
    - Formation of color centers
  - Can cause catastrophic faileure of resonator in oscillator
  - Can cause damage to turnig mirror in amplifiers

LINEAR HARMONIC GENERATION

- Process different for planar & helical wigglers
- Sensitive to Energy Spread
- Helical Wigglers
  - Phase matching of circularly polarized wave and helical beam rotation
    - High gains even when a_w/γ is small
  - Generates off-axis modes
- Planar Wigglers
  - Need a_w/γ large for substantial gain
  - Due to oscillatory nature of axial velocity

$$\mathbf{v} = \frac{a_w}{\gamma}\,\hat{\boldsymbol{e}}_x \cos k_w z + \upsilon_z \hat{\boldsymbol{e}}_z$$

$$\frac{\upsilon_z}{c} = \sqrt{1 - \frac{1 + a_w^2/2}{\gamma^2} - \frac{a_w^2}{2\gamma^2}\cos 2k_w z} \cong \frac{\bar{\upsilon}_z}{c} - \frac{a_w^2}{4\gamma^2}\cos 2k_w z$$

NONLINEAR HARMONIC GENERATION

The radiation depends on the source current $\mathbf{J} = -en\mathbf{v}$, where the density $n = n^{(0)} + n^{(1)} + \ldots + n^{(n)}$ and the velocity $\mathbf{v} = \mathbf{v}^{(0)} + \mathbf{v}^{(1)} + \ldots + \mathbf{v}^{(n)}$ and the expansion is in powers of the electromagnetic field **E**.

Continuity: convolution between density & velocity bunching

$$\frac{\partial}{\partial t} n^{(n)} + \nabla \cdot \sum_{i=0}^{n} n^{(i)} \mathbf{v}^{(n-i)} = 0$$

Electron Dynamics: relativistic effects

$$\gamma m_e \frac{d\mathbf{v}}{dt} = -e\left(1 - \frac{\mathbf{v}\mathbf{v}}{c^2}\right)\mathbf{E} - e\frac{\mathbf{v}}{\mathbf{c}} \times \left(\mathbf{B}_w + \mathbf{B}\right)$$

$$\frac{d\gamma}{dt} = -\frac{e}{m_e c^2}\mathbf{v} \cdot \mathbf{E}$$

Operative in all FEL configurations: amplifiers, oscillators, SASE, optical klystrons, and HGHG.

NONLINEAR HARMONIC GROWTH

- Because it depends on fundamental bunching, it is less sensitive to beam quality (emittance & energy spread) than the linear harmonic process.

- The source current at the harmonics varies as $\mathbf{J} \propto \mathbf{E}^h$, if $\mathbf{E} \propto e^{\Gamma z}$, then the harmonic growth rate varies as $\Gamma_h \propto h\Gamma$.
  - This leads to extremely rapid growth

- The power levels can be substantial with the 3rd harmonic reaching powers of as much as ≤ 1% of the fundamental and the 5th harmonic at 0.1% of the fundamental.

Implicitly included in non-KMR formulation

NONLINEAR HARMONICS SIMULATIONS

NHG has been observed in several SASE FELs (LEUTL, TESLA, VISA). MEDUSA has been used to simulate harmonic growth for sample LEUTL parameters, and the results are shown at the right.

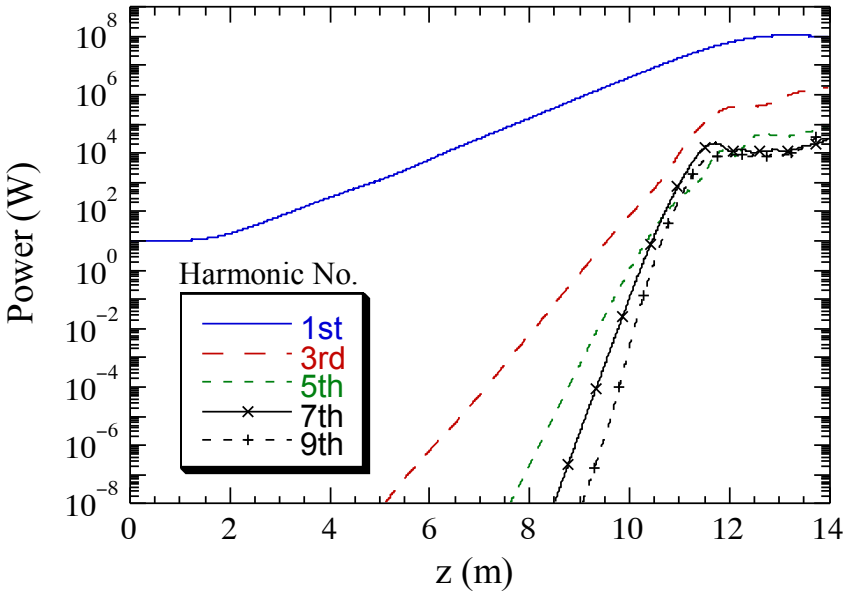

Harmonic No.	Gain Length (m)	Power
1	0.619	110 MW
2	0.364	189 kW
3	0.217	2.67 MW
4	0.166	84.3 W
5	0.128	103 kW
6	0.115	195 W
7	0.092	49.5 kW
8	0.079	478 W
9	0.072	50.0 kW

The gain length scales inversely with the harmonic number as expected, and substantial harmonic power levels are predicted.

NONLINEAR HARMONICS IN FEL OSCILLATORS

Nonlinear harmonics have been studied in SASE & HGHG FELs, but not in oscillators. MEDUSA can be used to study steady-state oscillators by generating a drive curve of output power versus input power. Since mirror loading is an issue and short Rayleigh range oscillators are under consideration, we take as our test case:

Energy	140 MeV
Peak Current	800 Amps
Normalized Emittance	1.9 microns
Peak on-Axis Wiggler Amplitude	10.1 kG
Wiggler Period	3.0 cm
Wiggler Length	20 λ_w
Fundamental Wavelength	1.04 microns
Rayleigh Range	1.93 cm

Parameters taken from an earlier study by Colson, Todd, and Neil

NONLINEAR HARMONIC PERFORMANCE

The gain at the fundamental and the powers in the 3rd and 5th harmonics versus input power at the fundamental are shown at right. Saturation occurs when the gain equals the mirror losses.

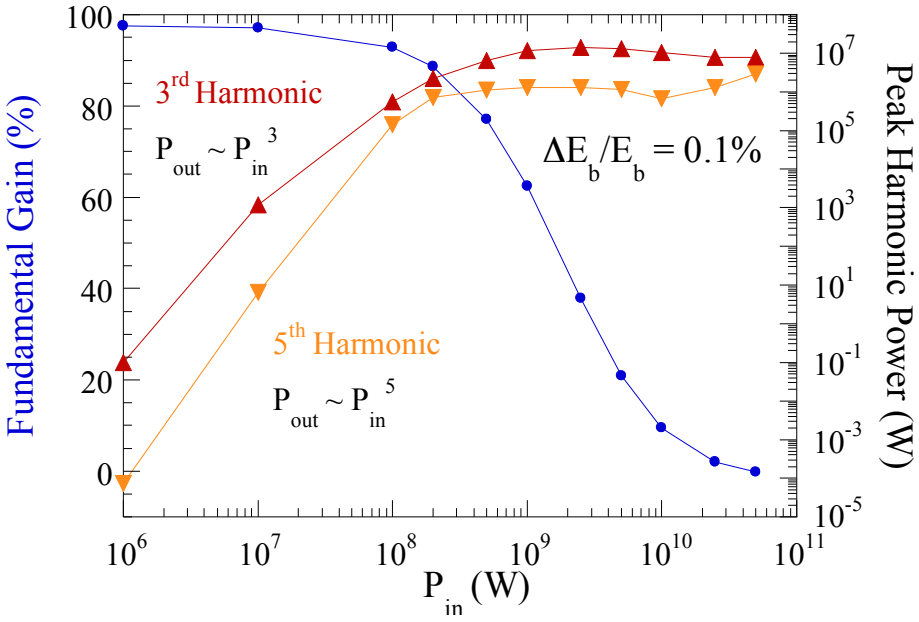

To get the harmonic power find the drive power where the gain equals the mirror losses. We find that:

- For 20% output coupling, the peak powers on the mirrors are about 5 GW at the fundamental, 13 MW at the 3rd harmonic, and 1.6 MW at the 5th harmonic.
- For a duty factor of 0.1%, this leads to average powers of 5 MW at the fundamental and 13 kW & 1.6 kW at the harmonics.

CONCLUSIONS ON NHG IN FEL OSCILLATORS

The oscillator results are consistent with those for the amplifier in that:

- The power for the harmonics in the unsaturated regime scales as the fundamental power raised to the h^{th} power.
- The saturated power at the 3rd harmonic is £ 1% that of the fundamental, and at the 5th harmonic it is ³ 0.1% that of the fundamental.
- For the case under study, these harmonic power levels occur for output coupling £ 40% and fundamental powers ³ 3 GW. This would provide for an FEL in the multi-MW class.
- The harmonic powers decline, and peak 5th harmonic powers in excess of 100 kW is expected for energy spreads £ 0.5%.
- **Not a show stopper**, but NHG must be taken into consideration in designing high–average power FELs

  → may need to go to helical wigglers

RUN MOVIES

DISTRIBUTION A

CODE VALIDATION AND BENCHMARKS

- Benchmarks against other codes
  - GENESIS, TDA3D, GINGER, RON, PERSEO
  - Amplifier/Oscillator (OPC)
- ELF Experiment at LLNL (35 GHz Amplifier)
- THz SASE Experiment at MIT (500 GHz)
- Reversed-Field FEL at MIT (35 GHz Amplifier)
- 2^{nd} Harmonic Oscillator Experiment at Jefferson Laboratory
  - 2^{nd} harmonic generated by configuring the resonator for off-axis modes
- High Gain Harmonic Generation Experiment at BNL (5.3 microns)
- Energy detuned Amplifier at BNL (794 nm)
- Tapered wiggler Amplifier at BNL (794 nm)

MEDUSA1D/PERSEO – START-UP FROM NOISE

MEDUSA1D & PERSEO show good agreement despite radically different formulations. The example corresponds to a full SASE simulation. The 5th harmonic spectrum is similarly close.

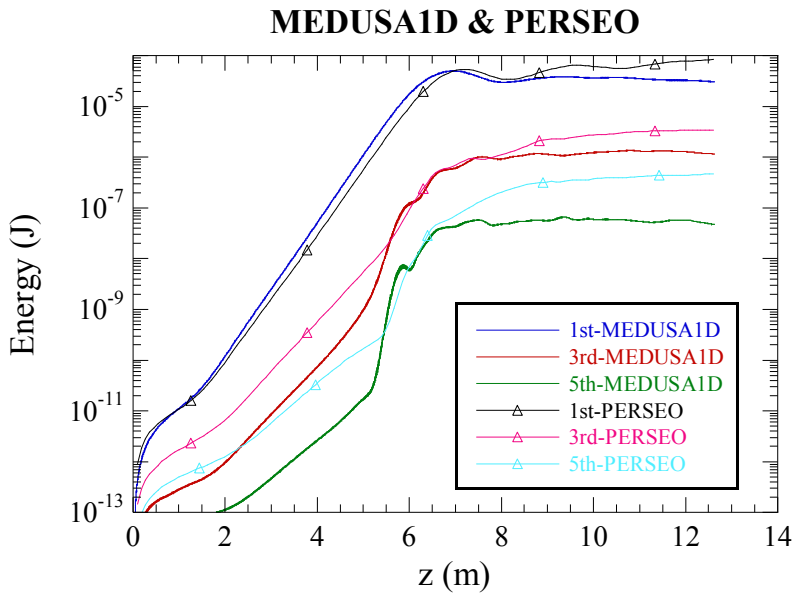

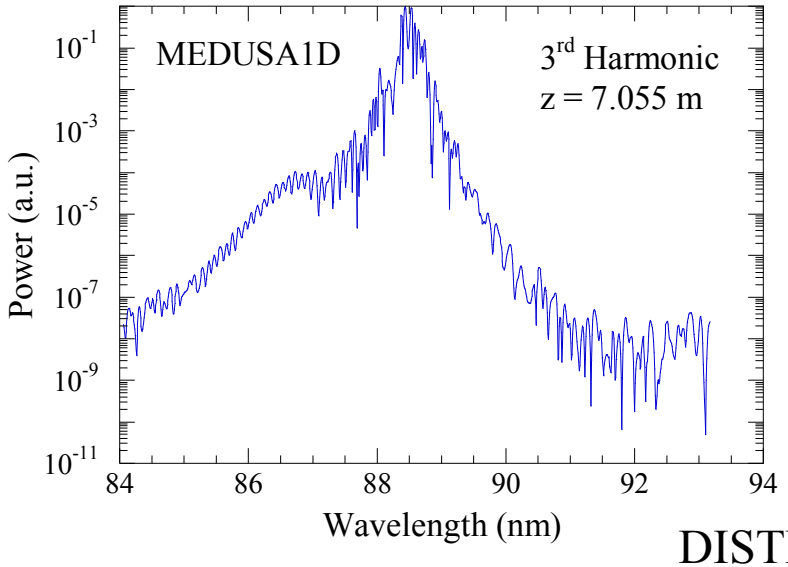

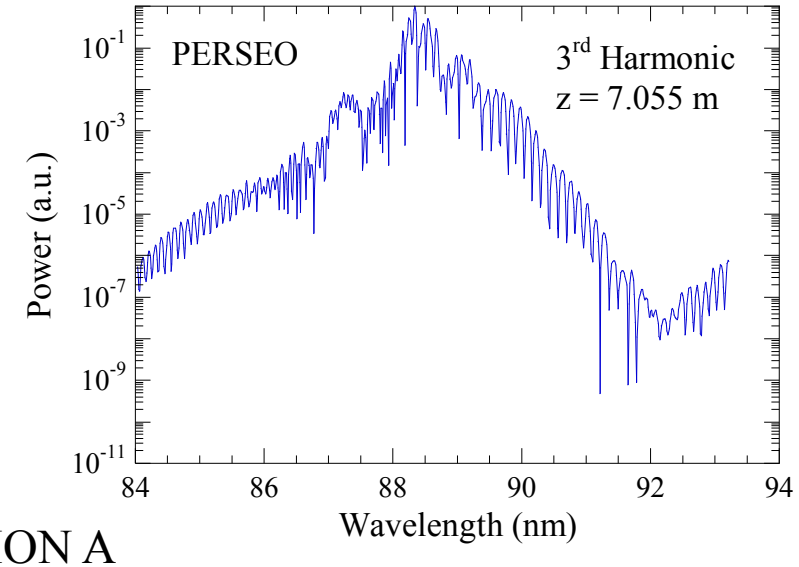

MEDUSA/MEDUSA1D/PERSEO

MEDUSA1D & PERSEO have 3-dimensional correction factors for diffraction/guiding and emittance as an option, and agreement is reasonably good

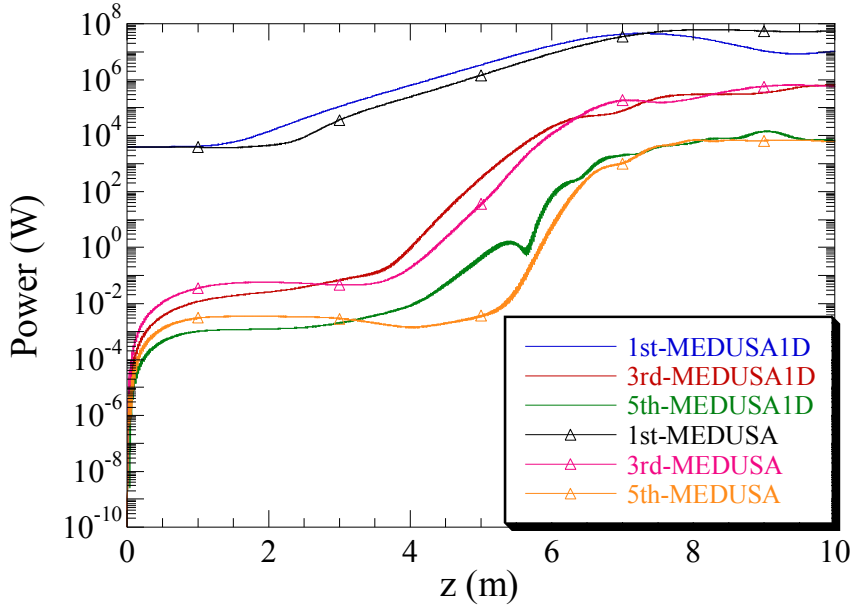

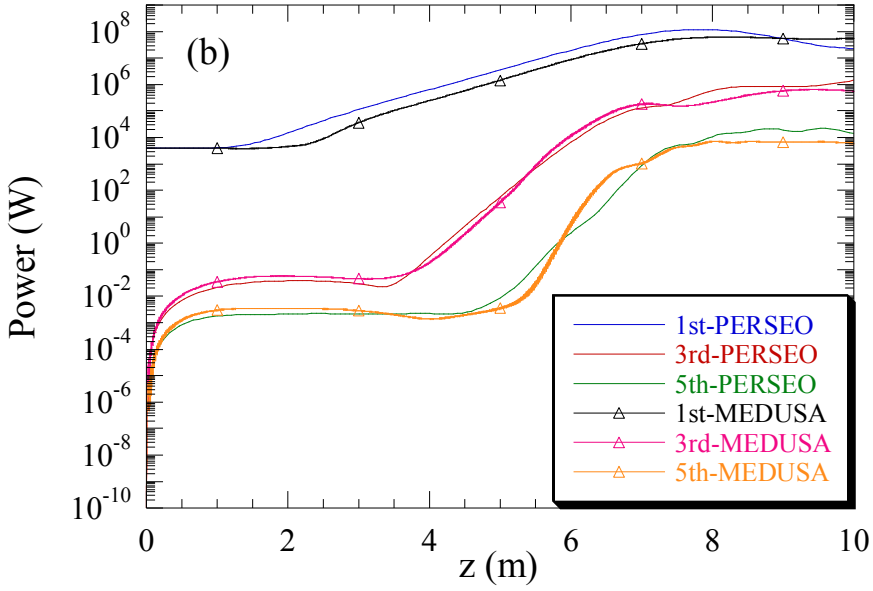

The 1-D codes can do some parameter scans quickly, but are not a substitute for full 3-D simulations.

DISTRIBUTION A

COMPARISONS: GINGER, GENESIS, TDA3D, RON

Some **MEDUSA** development (version 2) was funded by Argonne National Lab, which was interested in a code comparison for further analysis of x-ray FEL concepts.

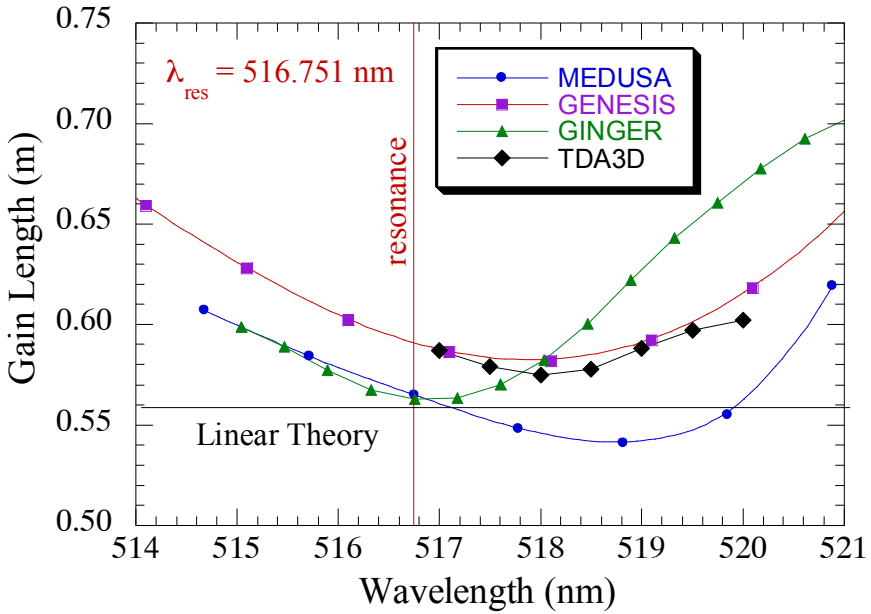

ELSEVIER
Nuclear Instruments and Methods in Physics Research A 445 (2000) 110–115
NUCLEAR INSTRUMENTS & METHODS IN PHYSICS RESEARCH Section A
www.elsevier.nl/locate/nima

Multi-dimensional free-electron laser simulation codes: a comparison study☆

S.G. Biedron[a,*], Y.C. Chae[a], R.J. Dejus[a], B. Faatz[b], H.P. Freund[c], S.V. Milton[a], H.-D. Nuhn[d], S. Reiche[b]

[a]Advanced Photon Source, Argonne National Laboratory, 9700 S.Cass Avenue, Argonne, IL 60439, USA
[b]Deutsches Elektronen Synchrotron, Notkestrasse 85, 22603 Hamburg, Germany
[c]Science Applications International Corporation, McLean, VA 22101, USA
[d]Stanford Linear Accelerator Center, Stanford, CA 94309, USA

Abstract

A self-amplified spontaneous emission (SASE) free-electron laser (FEL) is under construction at the Advanced Photon Source (APS). Five FEL simulation codes were used in the design phase: GENESIS, GINGER, MEDUSA, RON, and TDA3D. Initial comparisons between each of these independent formulations show good agreement for the parameters of the APS SASE FEL.

The codes were in generally good agreement, but they did not yield identical results, as shown in the tuning curve at left.

CODE COMPARISONS – POWER vs DISTANCE

The four nonlinear codes were in good agreement near resonance for single-segment and a multi-segment cases. Difference may be due to the discrepancies in the previous figure concerning the resonance.

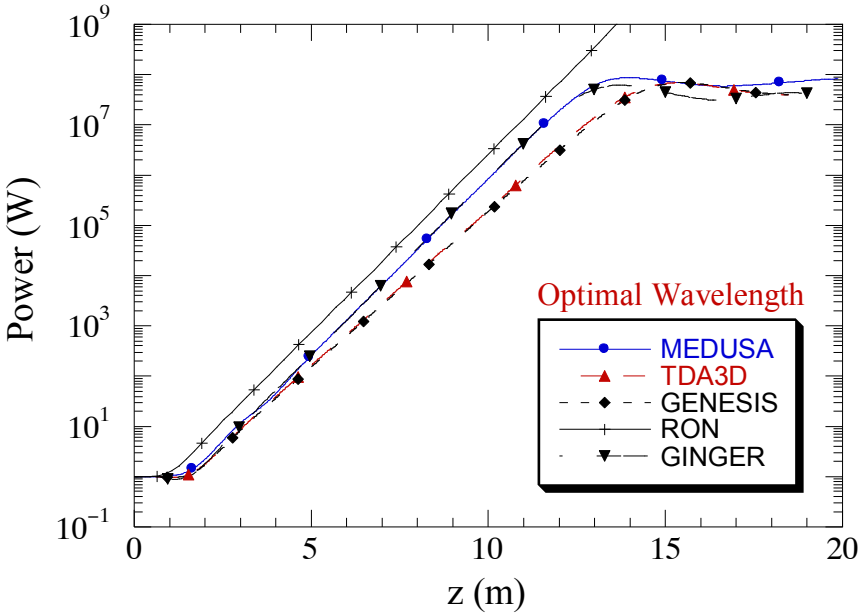

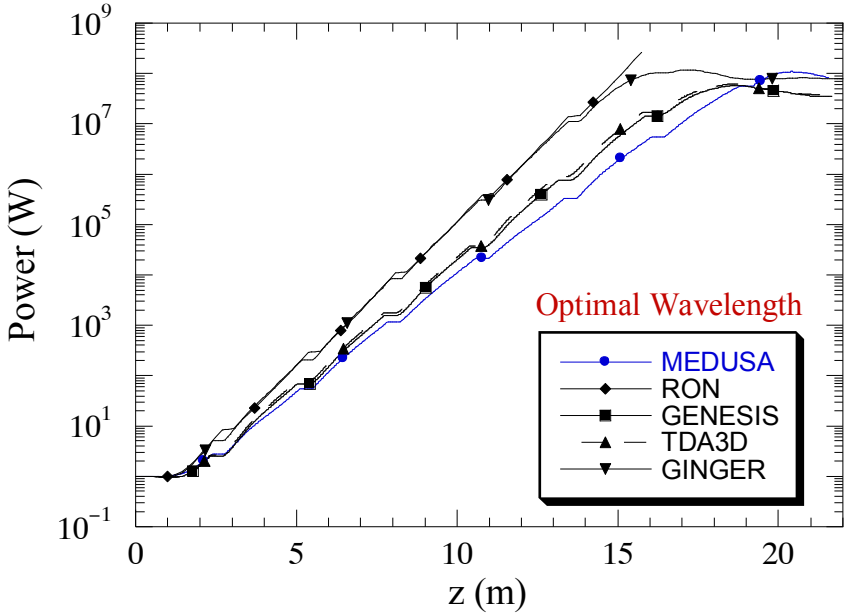

Code	Single-Segment		Multi-Segment	
	L_{sat}(m)	P_{sat} (MW)	L_{sat}(m)	P_{sat} (MW)
GENESIS	15.5	69	18.8	58
GINGER	13.7	62	17.2	120
MEDUSA	14.0	87	20.8	110
TDA3D	15.4	69	18.7	110

CODE COMPARISONS – GAIN LENGTH SCALING

Comparisons of the codes and with a linear analytic theory showed good agreement for the scaling of the gain length at resonance with emittance, peak current, and energy spread.

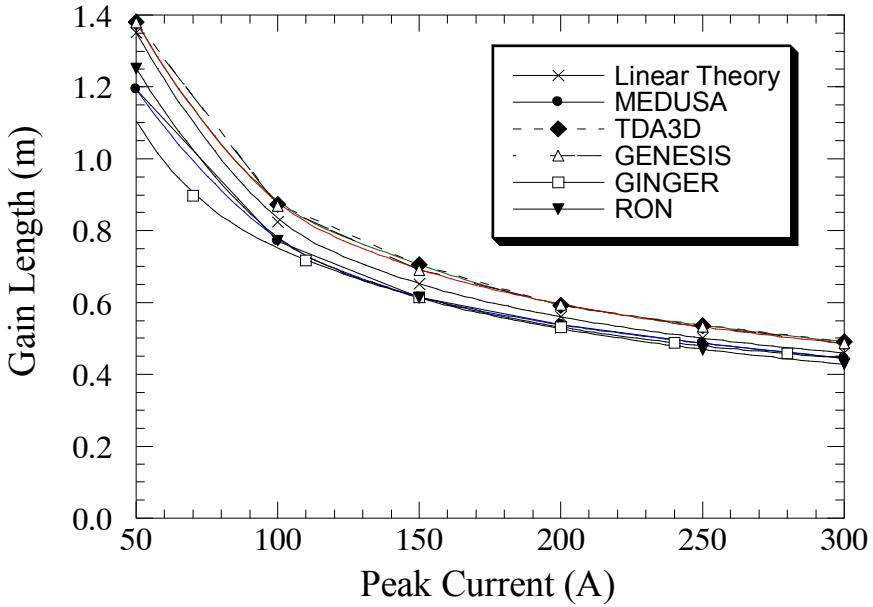

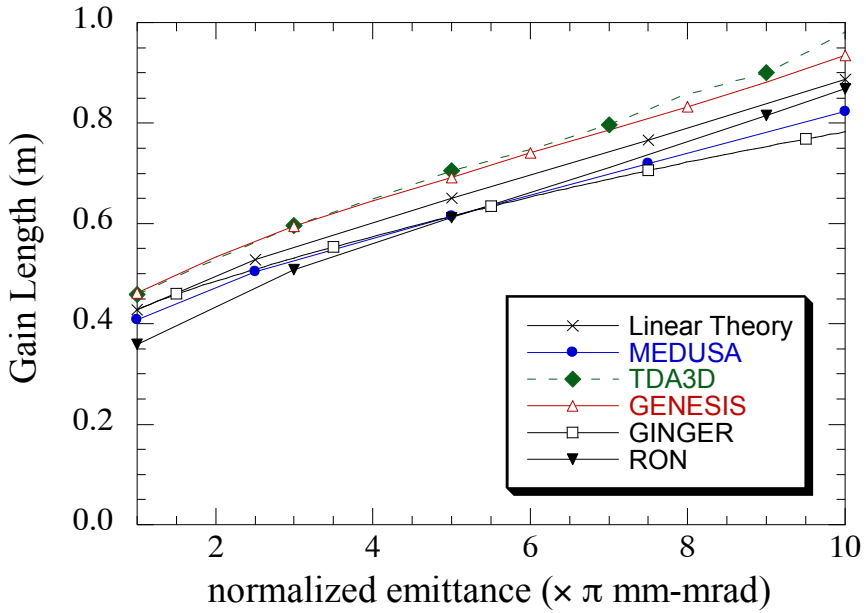

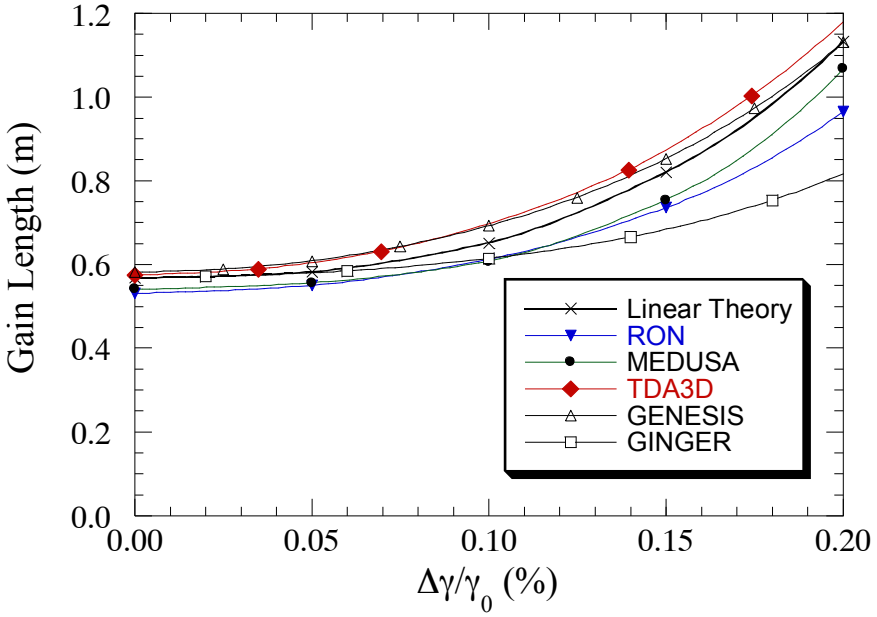

CODE COMPARISONS – WIGGLER ERRORS

At the time of the study, only MEDUSA, GENESIS, and TDA3D included a model for wiggler imperfections. These three codes were run to compare these models for the single-segment case.

Reasonable agreement was found for the codes. The differences between TDA3D and GENESIS here were surprising since these codes are siblings; however, the differences are not large for any of the codes.

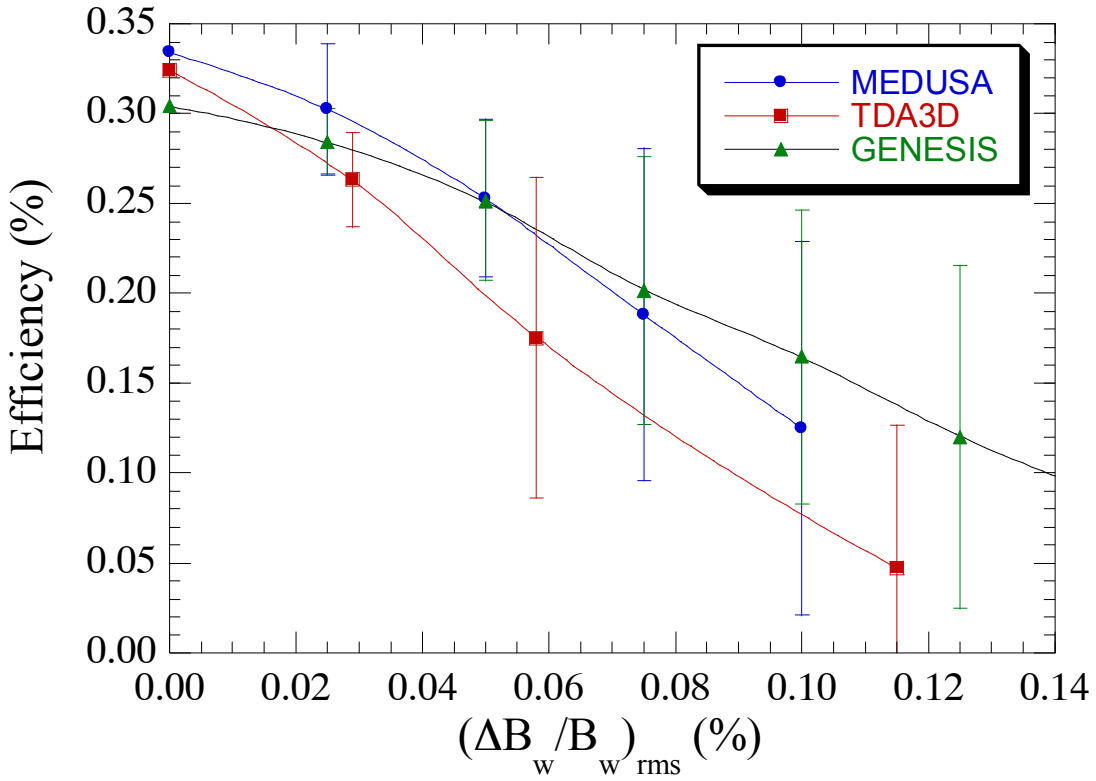

ELF EXPERIMENT AT LLNL

This experiment was a 34.6 GHz amplifier using the ETA induction linac at LLNL and a planar wiggler. It achieved a peak output power of 1 GW for an efficiency of 35% with a tapered wiggler. The parameters were:

Wiggler Amplitude	3.72 kG
Wiggler Period	9.80 cm
Wiggler Taper	55%
Taper Length	1.1 m
Beam Energy	3.5 MeV
Beam Current	850 A
Beam Radius	1.0 cm
Energy Spread	< 2.0%

1 m Segment of the ELF Wiggler

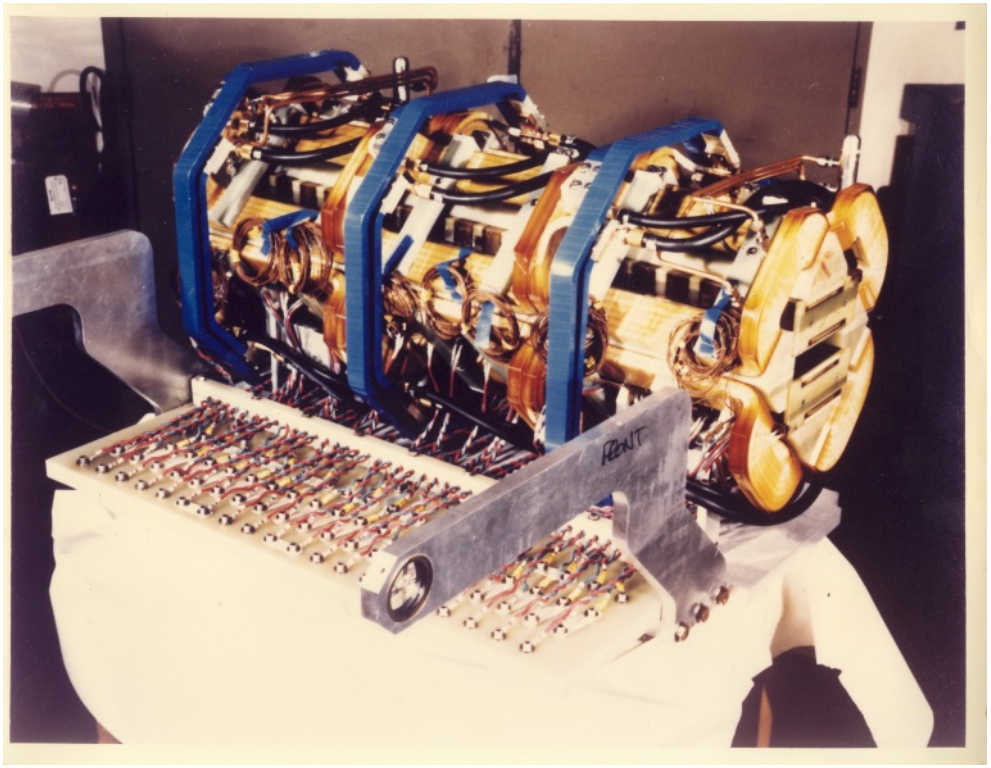

ELF POWER COMPARISON

VOLUME 57, NUMBER 17 PHYSICAL REVIEW LETTERS 27 OCTOBER 1986

High-Efficiency Extraction of Microwave Radiation from a Tapered-Wiggler Free-Electron Laser

T. J. Orzechowski, B. R. Anderson, J. C. Clark, W. M. Fawley, A. C. Paul, D. Prosnitz, E. T. Scharlemann, and S. M. Yarema
Lawrence Livermore National Laboratory, University of California at Livermore, Livermore, California 94550

and

D. B. Hopkins, A. M. Sessler, and J. S. Wurtele
Lawrence Berkeley Laboratory, University of California, Berkeley, California 74720
(Received 4 August 1986)

We have substantially increased the output power and extraction efficiency of a free-electron laser operating at 34.6 GHz by tapering the wiggler magnetic field. In the exponential-gain regime, the laser exhibited a measured gain of 34 dB/m. With a 50-kW input signal, the amplifier saturated in 1.3 m with a 180-MW output signal. By using a taper that brought the magnetic field at the end of the wiggler down to 45% of its initial (peak) value, we increased the output signal to 1.0 GW. This corresponds to an extraction efficiency of 34%.

LLNL reported observing 1 GW after tapering the wiggler downward by 55% over a length of 1.1 m.

WIGGLIN was designed to treat this geometry and showed good agreement with the measured power using an energy spread of 1.5%. This was close to the best "guess" that LLNL could provide. **WIGGLIN** reproduced the output power to within an embarrassingly small discrepancy with the experiment.

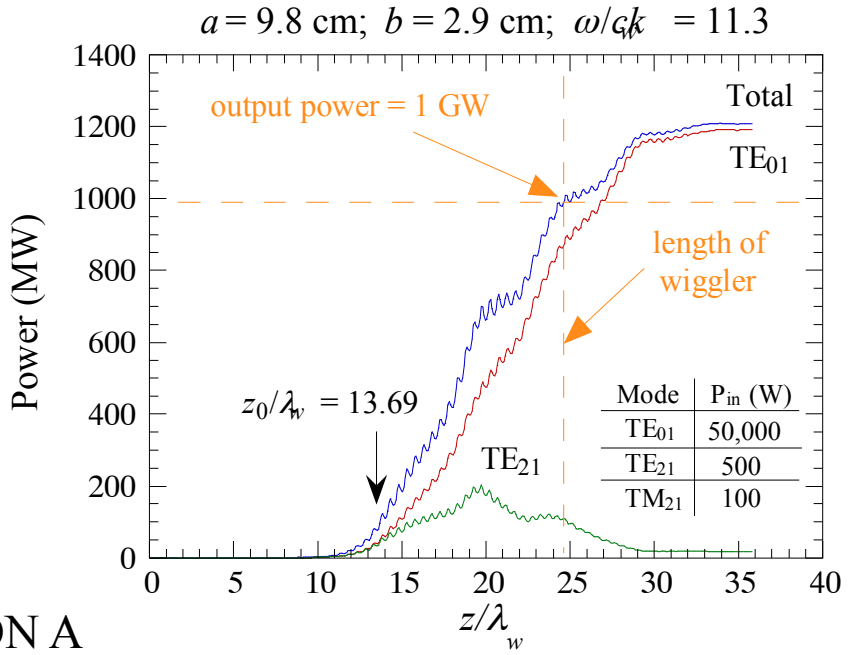

ELF TUNING COMPARISON

150 Nuclear Instruments and Methods in Physics Research A250 (1986) 150–158
North-Holland, Amsterdam

COMPARISON OF THE LIVERMORE MICROWAVE FEL RESULTS AT ELF WITH 2D NUMERICAL SIMULATION

E.T. SCHARLEMANN, W.M. FAWLEY, B.R. ANDERSON ** and T.J. ORZECHOWSKI
*Lawrence Livermore National Laboratory *, Livermore, CA 94550, USA*

The experimental results of the ELF microwave free electron laser experiment are compared with 2D numerical simulations using the LLNL code FRED. The data comprise (1) microwave power vs wiggler magnetic field at fixed wiggler length, (2) microwave power vs wiggler length at fixed wiggler field, and (3) relative power in the two waveguide modes that couple strongly to the electrons, vs wiggler length.

The code evolves the electrons' energies and ponderomotive phases according to the averaged single-particle equations derived by Kroll, Morton and Rosenbluth, and the fields according to the paraxial wave equation with the source term as derived by Colson. The particle motion is fully three-dimensional. The field solver is two-dimensional, but because only the lowest mode is excited in the short waveguide dimension, the code is accurately three-dimensional for microwave simulations.

Longitudinal space-charge forces reduce the gain and increase the synchrotron period of the electrons (after saturation of the amplifier) by roughly 20%. Space-charge forces have been included in the code approximately (so that the running time of the code is not significantly increased), and bring experiment and theory into excellent agreement. The approximation used to add space-charge forces is described.

This was an amplifier driven by a fixed-frequency magnetron, so the tuning measurements were done by varying the wiggler field. Tuning data scanned from the paper at left, and the results from WIGGLIN were superimposed.

LLNL's in-house code (FRED) showed a discrepancy of about 7% from the measured data which was thought due to collective space-charge forces. I believe this conclusion was in error and due to deficiencies in FRED. WIGGLIN was only detuned by < 30 G from the experimental peak showing a discrepancy < 1% without inclusion of space-charge.

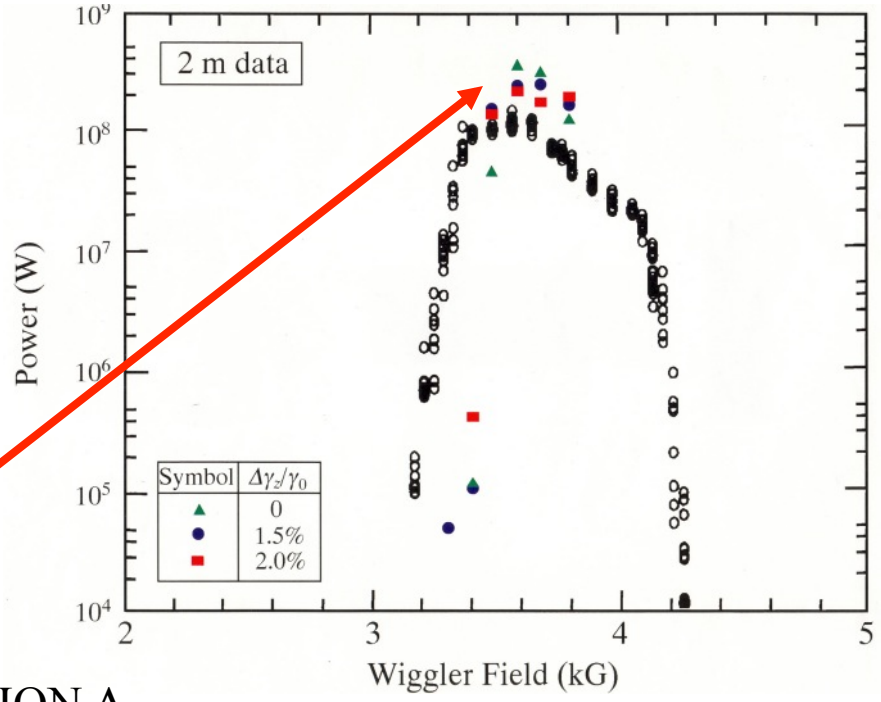

MIT 500 GHz SASE FEL EXPERIMENT

This was a THz SASE FEL in a cylindrical drift tube using a bifilar helical wiggler. As such, **A R A C H N E** was the appropriate code, and was found to be in good agreement with the experiment.

Phys. Fluids B 1 (7), July 1989 0899-8221/89/071511-08$01.90

A millimeter and submillimeter wavelength free-electron laser

D. A. Kirkpatrick,[a] G. Bekefi, and A. C. DiRienzo
Department of Physics and Research Laboratory of Electronics, Massachusetts Institute of Technology, Cambridge, Massachusetts 02139
H. P. Freund[a] and A. K. Ganguly
Naval Research Laboratory, Washington, D.C. 20375-5000

(Received 20 January 1989; accepted 28 March 1989)

Measurements of millimeter and submillimeter wavelength emission (240 GHz $< \omega/2\pi <$ 470 GHz) from a free-electron laser are reported. The laser operates as a superradiant amplifier and without an axial guide magnetic field; focusing and transport of the electron beam through the wiggler interaction region are achieved by means of the bifilar helical wiggler field itself. Approximately 18 MW of rf power has been observed at a frequency of 470 GHz, corresponding to an electronic efficiency of 0.8%. Frequency spectra are measured with a grating spectrometer and show linewidths $\Delta\omega/\omega \sim 2\%$–4%. The experimental results are in very good agreement with nonlinear numerical simulations.

Experimental Configuration

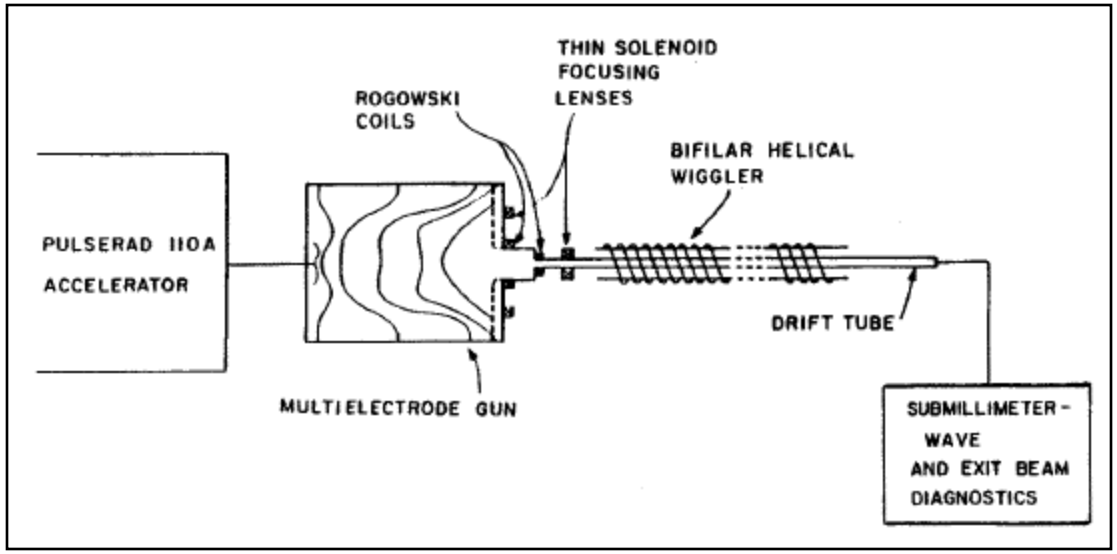

MIT/SASE BEAM ENERGY SPREAD DIAGNOSTIC

There was no good energy spread diagnostic for this experiment, only an indication from gun simulations (EGUN) that the energy spread was no higher than 0.25%.

Experiment

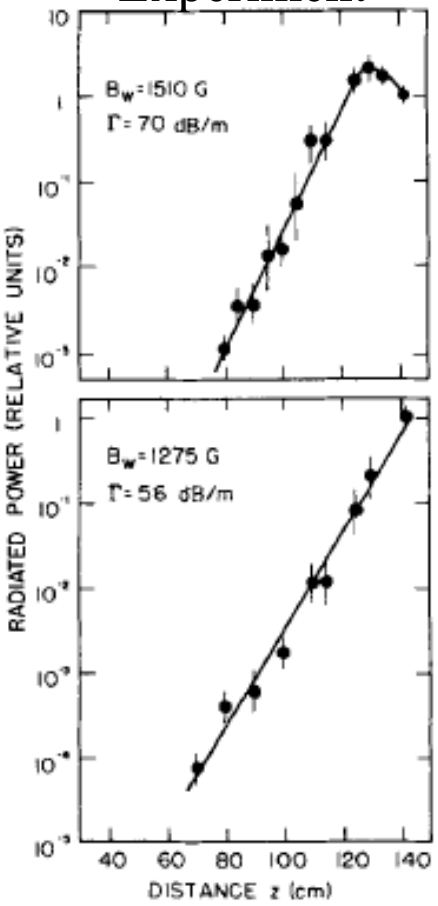

ARACHNE

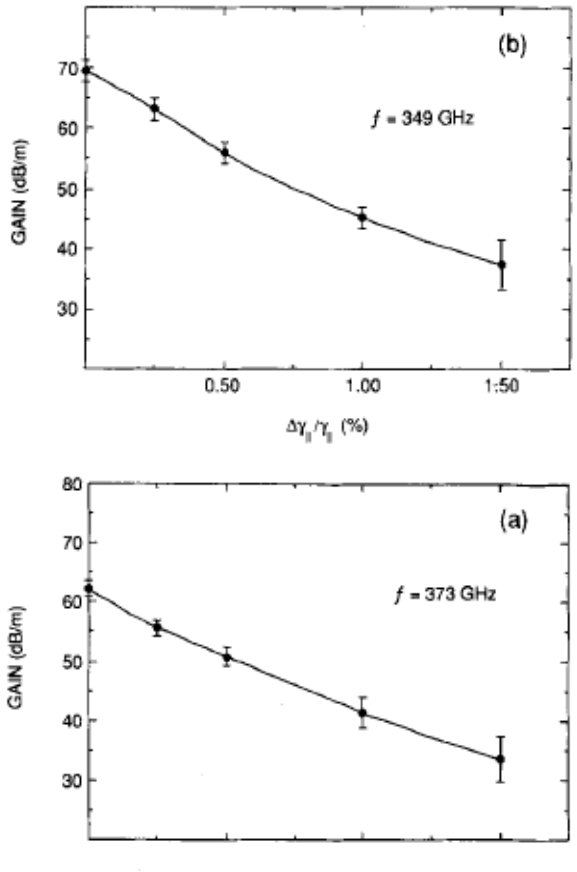

ARACHNE was run for a range of energy spreads corresponding to two different wiggler field strengths and frequencies, and the growth rates were compared. The results were consistent with the EGUN simulations.

→ Used to obtain spectrum

DISTRIBUTION A

MIT/SASE SPECTRAL COMPARISONS

ARACHNE reproduced the measured spectrum closely using the previously determined energy spread.

- These runs were made before the polychromatic feature was added, so that they were made one frequency at a time. This is valid since the FEL did not saturate for this case.
- Arbitrary units used since there was no good estimate of the start power.
- Absolute powers were also consistent as measured and simulated (13-18 MW).

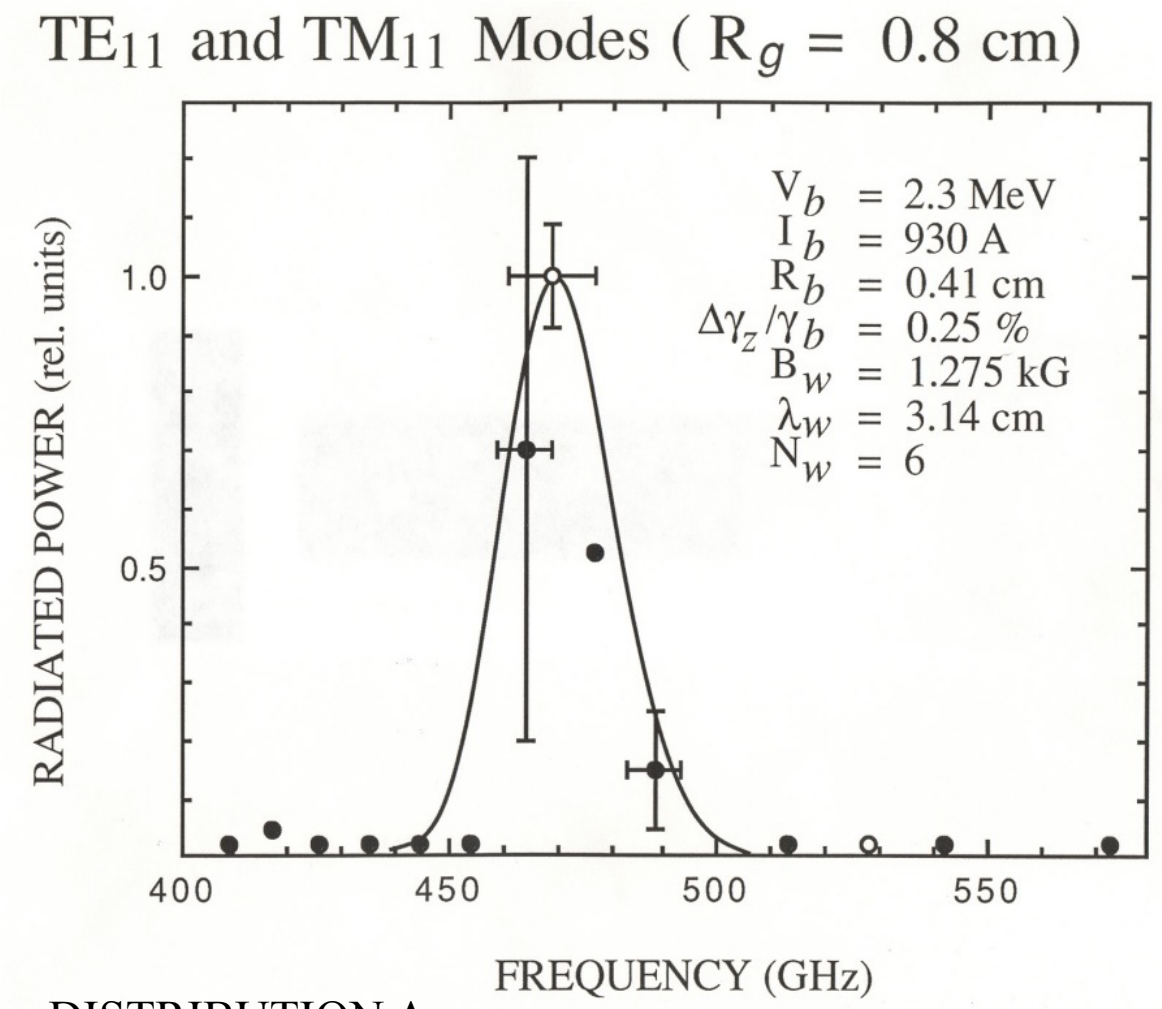

MIT REVERSED-FIELD FEL AMPLIFIER

This was a 35 GHz amplifier that achieved an efficiency of 27% without a tapered wiggler; thereby proving:

-- That you can do everything wrong, and still succeed --
(But you shouldn't count on it)

VOLUME 67, NUMBER 22 PHYSICAL REVIEW LETTERS 25 NOVEMBER 1991

Experimental Study of a 33.3-GHz Free-Electron-Laser Amplifier with a Reversed Axial Guide Magnetic Field

M. E. Conde and G. Bekefi
Department of Physics and Research Laboratory of Electronics, Massachusetts Institute of Technology, Cambridge, Massachusetts 02139
(Received 22 July 1991)

We report on a new regime of free-electron-laser operation with reversed axial guide magnetic field, in which the rotational motion of the electrons in the helical wiggler field is opposed by the presence of the uniform guide field. The 33.3-GHz free-electron-laser amplifier is driven by a mildly relativistic electron beam (750 kV, 300 A, 30 ns) and generates 61 MW of radiation with a 27% conversion efficiency. Measurements with the conventional orientation of the axial field show a considerable loss of power and efficiency.

Configuration: cylindrical drift tube with a helical wiggler and an axial guide field.

→ **ARACHNE** is the code of choice

AXIAL GUIDE FIELD EFFECTS ON THE FEL

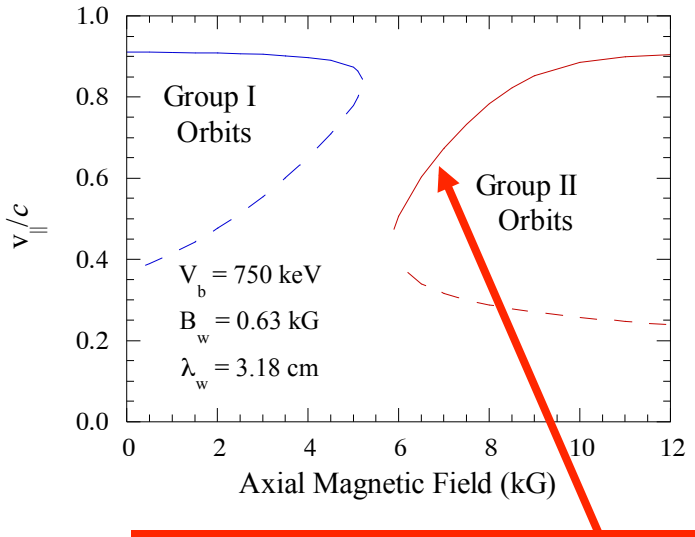

When the guide field and the wiggler field a directed in a parallel sense, then there is a magneto-resonance when the Larmor period coincides with the wiggler period. As this point is neared, the wiggle velocity increases as do the FEL gain and efficiency.

→ all previous FEL experiments dealt with this configuration

Original Goal of the Experiment

Negative-mass regime where the beam accelerates axially as the total energy decreases → enhanced efficiencies seen in simulation (**ARACHNE**)

There is no corresponding magneto-resonance when the guide field is directed anti-parallel to the wiggler.

→ not thought to be an interesting regime for study

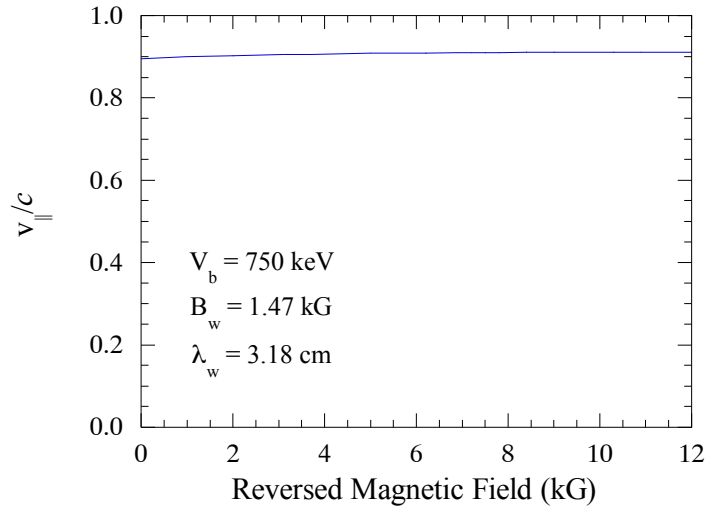

MIT REVERSED-FIELD FEL CONFIGURATION

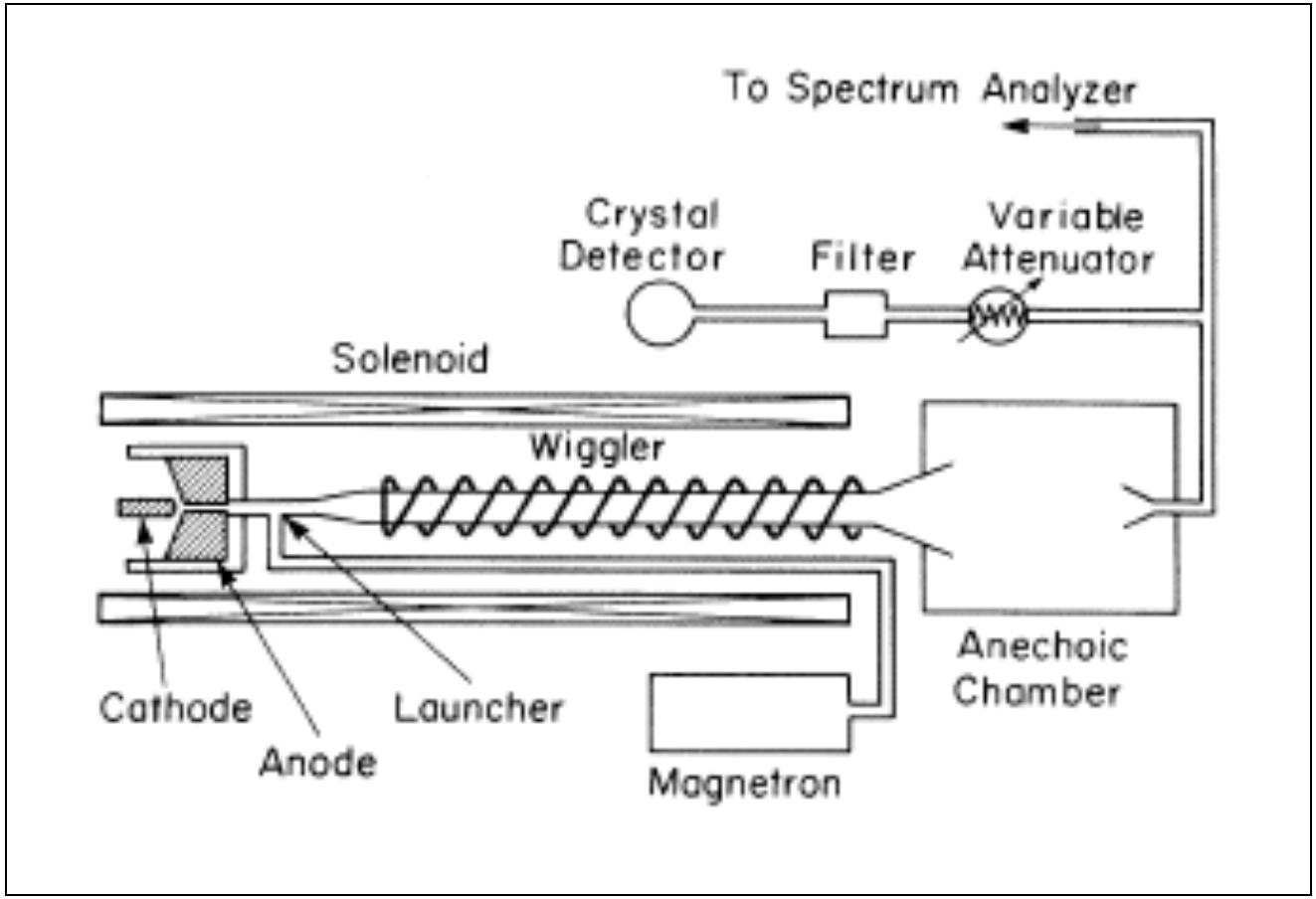

Hardware: borrowed from several previous FELs

- Accelerator – Pulserad 110A used in 500 GHz SASE experiment
- Wiggler – Wound for the 500 GHz SASE experiment
- Magnetron – Used for the ELF amplifier at LLNL

AMPLIFIER PERFORMANCE COMPARISON

The experimenters were originally **unaware** that:

(1) they had a **left-handed wiggler**

(2) their beam voltage was 750 keV. **They believed their beam voltage was 1.2 MeV.**

→ FEL resonance in Group II orbits at 35 GHz

•When the polarization of the wiggler was realized, they had to re-check the calibration of the beam voltage.

• This process involved feedback from ARACHNE, which was found to be in close agreement with the observed performance.

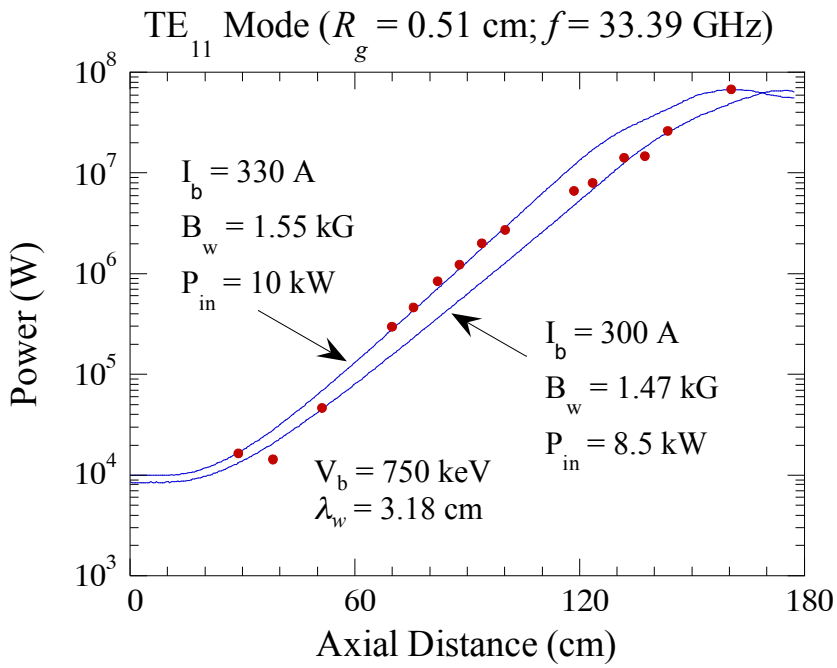

ANTI-RESONANT POWER HOLE

An unexpected experimental result was that a "power hole" was found near the anti-resonance. This behavior was completely unexpected since there was not believed to be any unusual orbital properties associated with the anti-resonance. The power hole, however, was reproduced in ARACHNE.

The cause of the power hole was identified as a wiggler-gradient driven orbital instability.

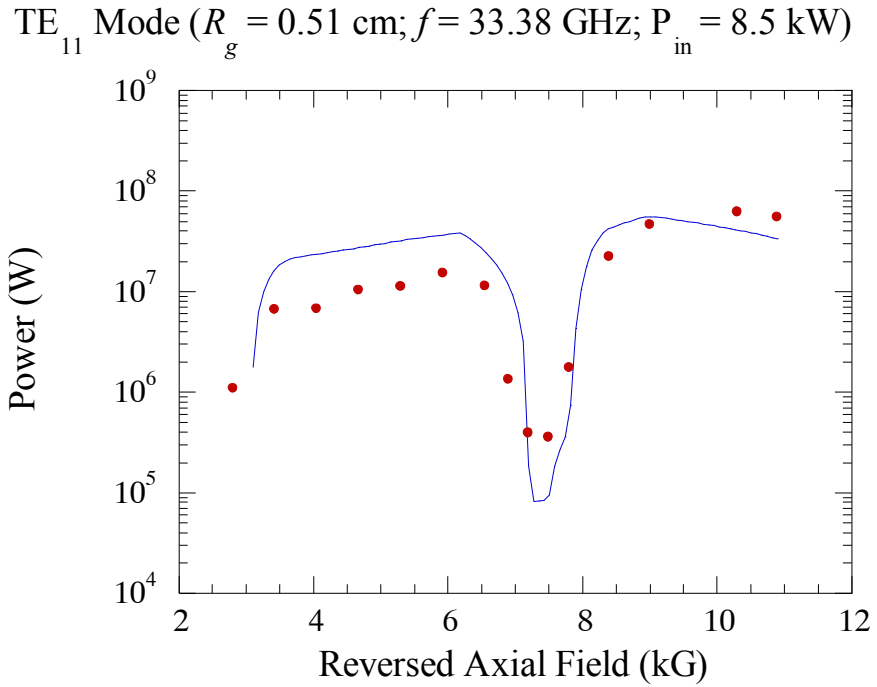

REVERSED FIELD ORBITAL INSTABILITY

There is a previously unsuspected anti-resonant driving force due to the wiggler inhomogeniety that affects orbits near the edge of the beam, and drives them unstable

→ anti-resonant power hole

The effects of the orbital instability are implicitly included in the particle tracking algorithm in the MEDUSA family of codes

→ **ADVANTAGE:** FIRST PRINCIPLES PARTICLE TRACKING

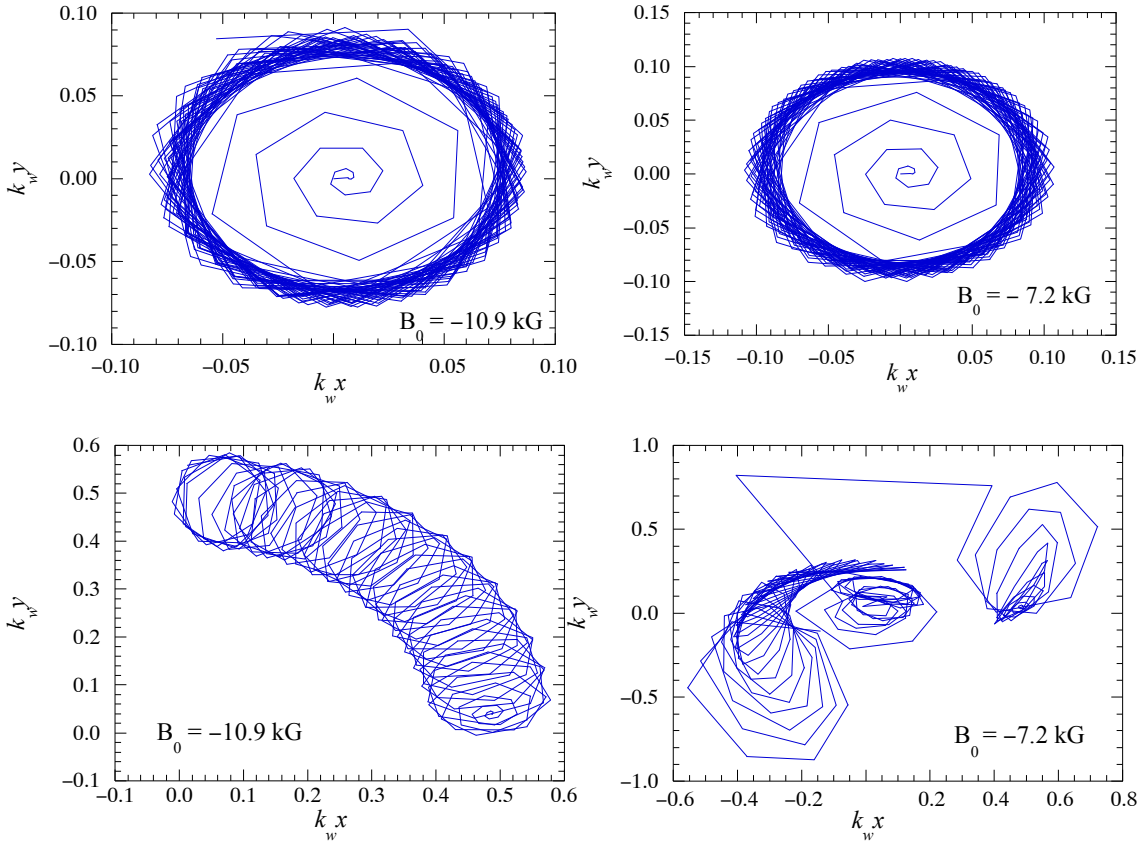

DISTRIBUTION A

2nd HARMONIC EXPERIMENT AT JEFFERSON LAB

The 2nd harmonic can grow in a planar wiggler FEL by exciting asymmetric modes. This is a linear mechanism, and is included in MEDUSA. This was studied for the Jefferson Lab FEL by creating a misalignment between the beam and the resonator axis.

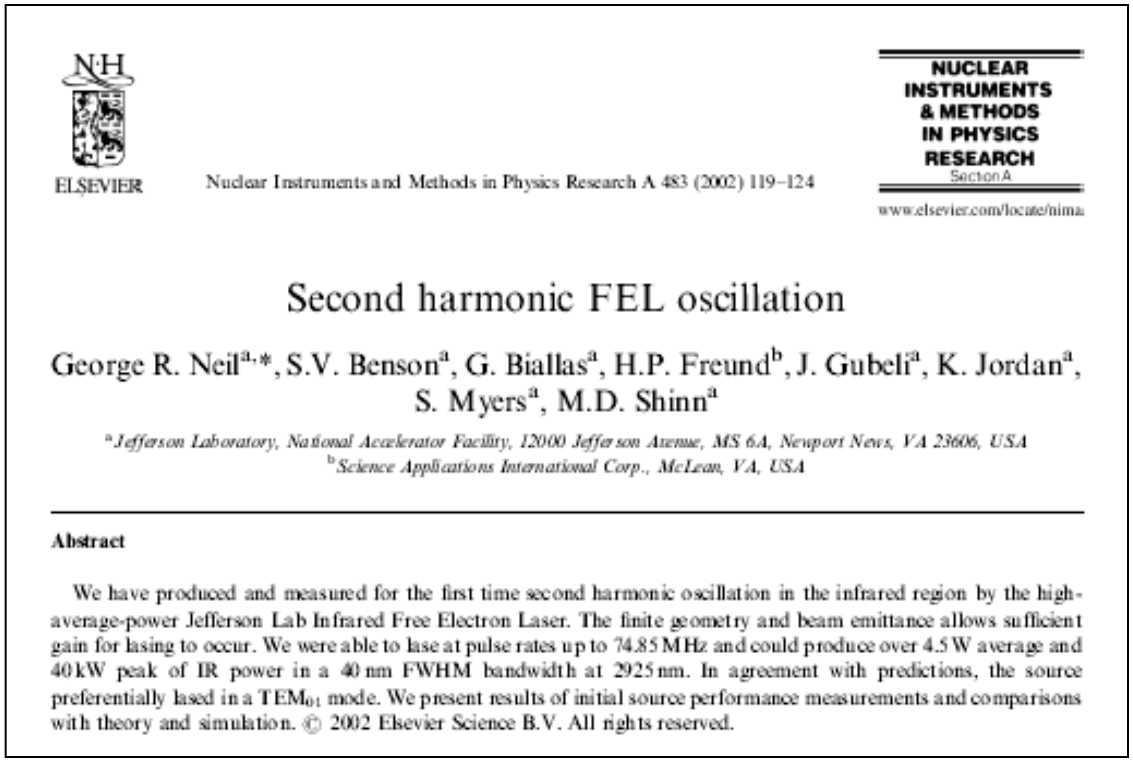

ELSEVIER

Nuclear Instruments and Methods in Physics Research A 483 (2002) 119–124

NUCLEAR INSTRUMENTS & METHODS IN PHYSICS RESEARCH Section A

www.elsevier.com/locate/nima

Second harmonic FEL oscillation

George R. Neil[a,*], S.V. Benson[a], G. Biallas[a], H.P. Freund[b], J. Gubeli[a], K. Jordan[a], S. Myers[a], M.D. Shinn[a]

[a] *Jefferson Laboratory, National Accelerator Facility, 12000 Jefferson Avenue, MS 6A, Newport News, VA 23606, USA*
[b] *Science Applications International Corp., McLean, VA, USA*

Abstract

We have produced and measured for the first time second harmonic oscillation in the infrared region by the high-average-power Jefferson Lab Infrared Free Electron Laser. The finite geometry and beam emittance allows sufficient gain for lasing to occur. We were able to lase at pulse rates up to 74.85 MHz and could produce over 4.5 W average and 40 kW peak of IR power in a 40 nm FWHM bandwidth at 2925 nm. In agreement with predictions, the source preferentially lased in a TEM_{01} mode. We present results of initial source performance measurements and comparisons with theory and simulation.

Note that this operates by a linear harmonic generation process.

SECOND HARMONIC IN THE JLAB FEL

Scans for the single-pass gain with variations in current and emittance were made using MEDUSA since there were uncertainties in these parameters. This would produce an operating window.

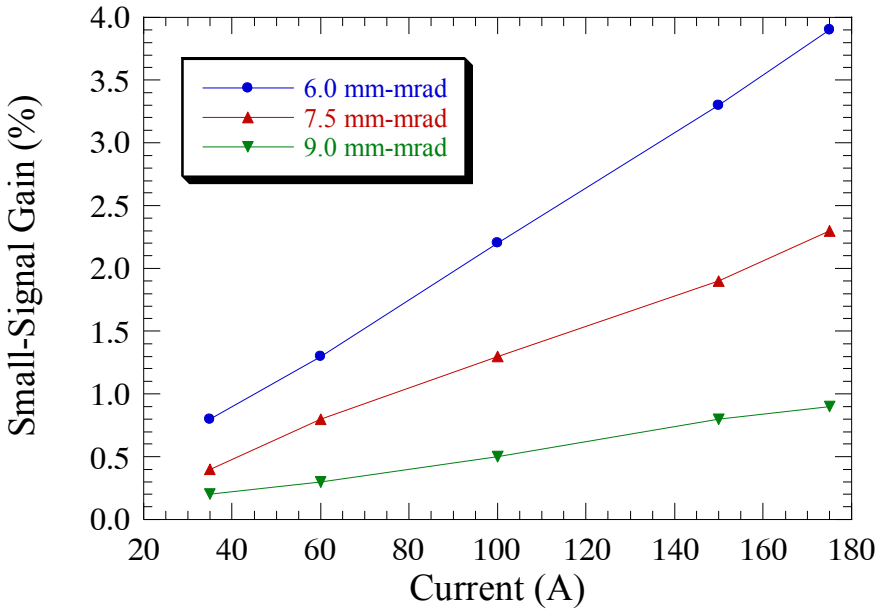

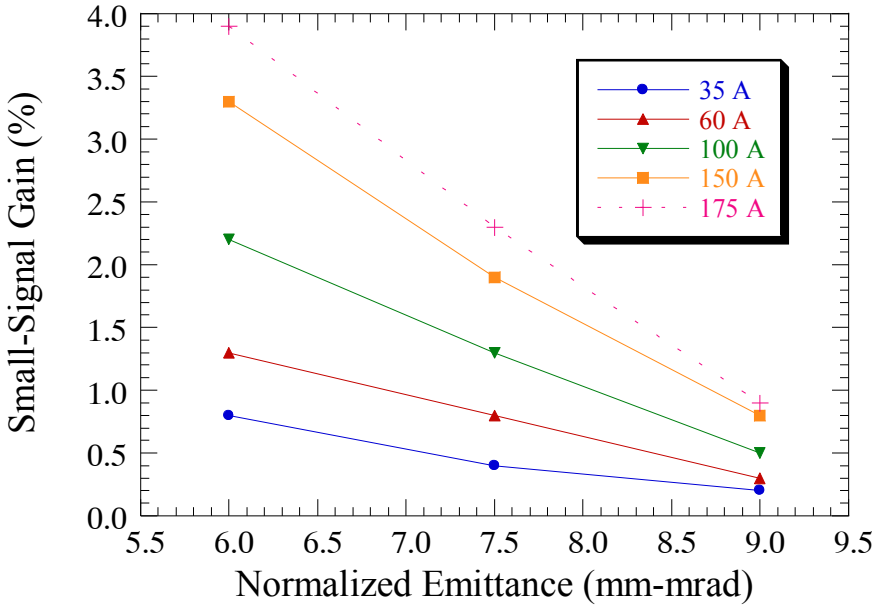

For the best estimate value of the beam parameters (60 A, 7.5 mm-mrad), **MEDUSA** predicts a small signal gain per pass of 0.8%. This is close to the **measured** value of 0.73% gain per pass.

SIMULATIONS OF THE HGHG EXPERIMENT

VOLUME 86, NUMBER 26 PHYSICAL REVIEW LETTERS 25 JUNE 2001

Characterization of a High-Gain Harmonic-Generation Free-Electron Laser at Saturation

A. Doyuran,[1] M. Babzien,[1] T. Shaftan,[1] L. H. Yu,[1] L. F. DiMauro,[1] I. Ben-Zvi,[1] S. G. Biedron,[2] W. Graves,[1] E. Johnson,[1] S. Krinsky,[1] R. Malone,[1] I. Pogorelsky,[1] J. Skaritka,[1] G. Rakowsky,[1] X. J. Wang,[1] M. Woodle,[1] V. Yakimenko,[1] J. Jagger,[2] V. Sajaev,[2] and I. Vasserman[2]

[1]*Brookhaven National Laboratory, Upton, New York 11973*

[2]*Advanced Photon Source, Argonne National Laboratory, Argonne, Illinois 60439*

(Received 18 January 2001)

We report on an experimental investigation characterizing the output of a high-gain harmonic-generation (HGHG) free-electron laser (FEL) at saturation. A seed CO_2 laser at a wavelength of 10.6 μm was used to generate amplified FEL output at 5.3 μm. Measurement of the frequency spectrum, pulse duration, and correlation length of the 5.3 μm output verified that the light is longitudinally coherent. Investigation of the electron energy distribution and output harmonic energies provides evidence for saturated HGHG FEL operation.

The HGHG experiment at Brookhaven National Laboratory bunched the beam using a seed laser at 10.6 microns, enhanced the bunching in a chicane, and then extracted power in a wiggler tuned to 5.3 microns.

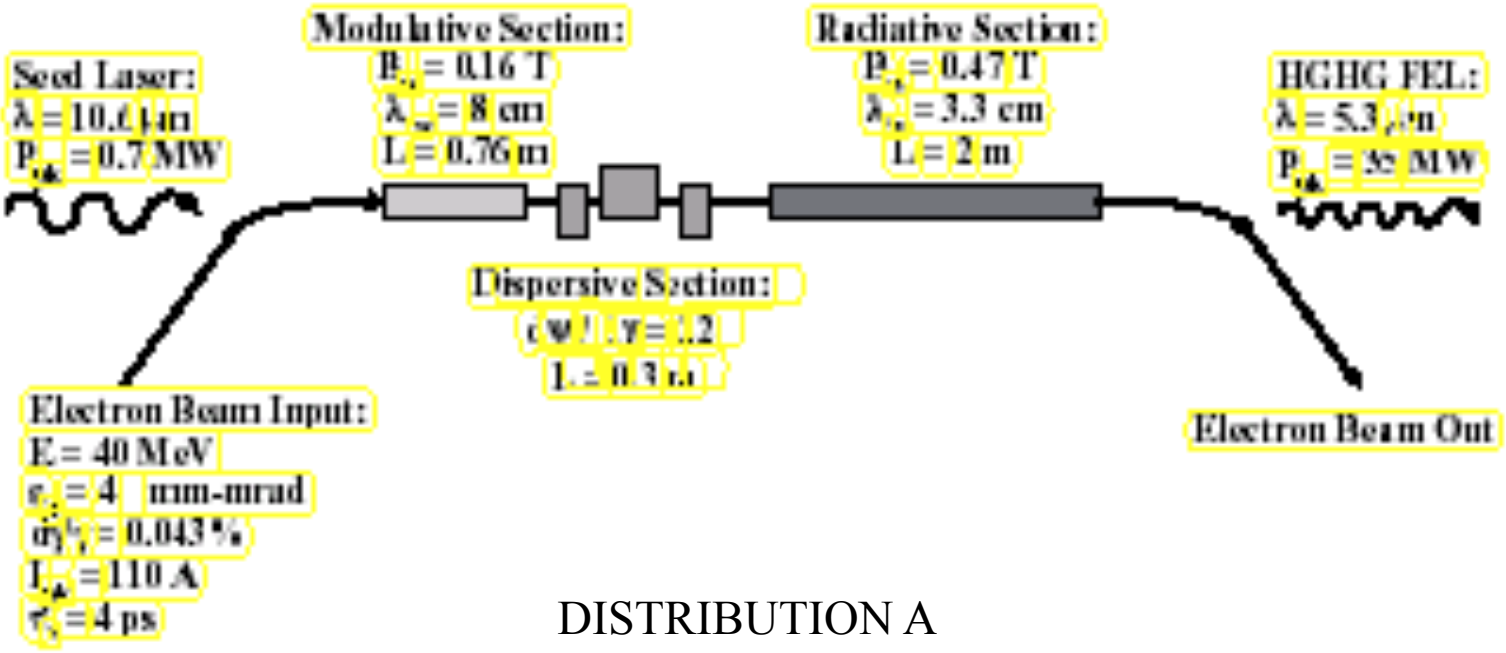

DISTRIBUTION A

ENHANCED BUNCHING IN THE CHICANE

• A velocity/phase modulation was imposed at 10.6 microns in the 1st wiggler which was enhanced in the chicane (like optical klystron)

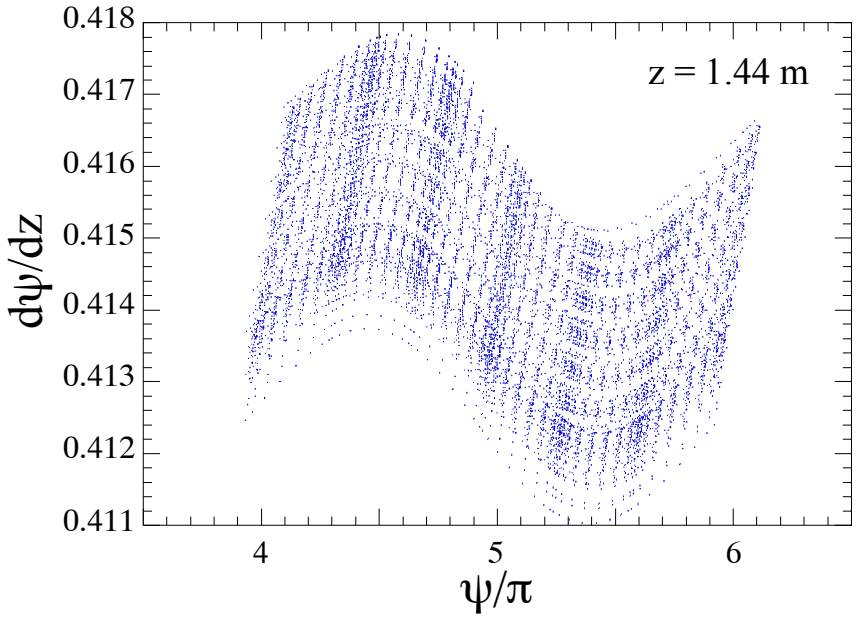

Before the chicane

After the chicane

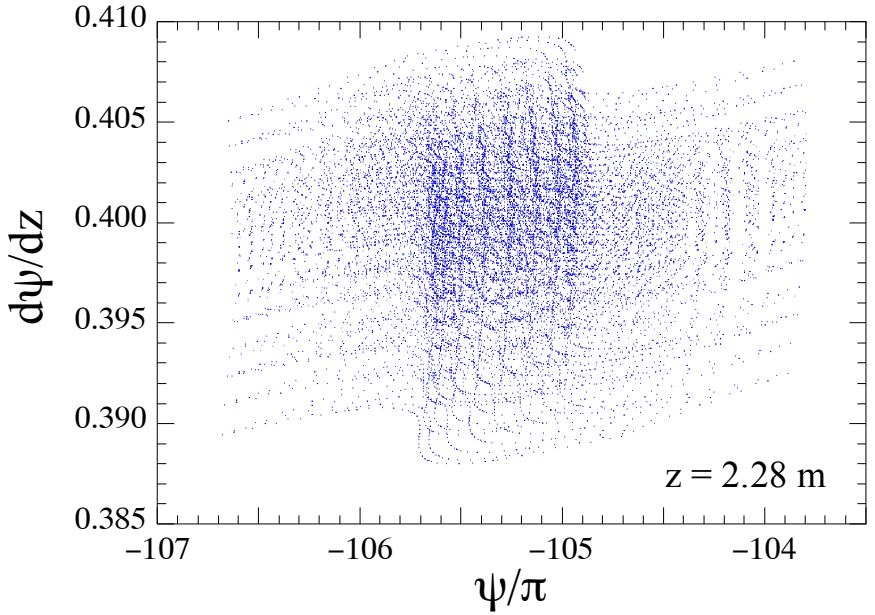

DISTRIBUTION A

HGHG/MEDUSA COMPARISONS

Simulations of the experiment using MEDUSA showed good agreement for the fundamental power (28 MW) and with the fractional powers at the 2nd & 3rd harmonics. Sample results for the 2nd and 3rd harmonics are shown at the left below

	$P_{harmonic}/P_{fundamental}$	
Harmonic	HGHG	MEDUSA
2	2.0×10^{-4}	6.0×10^{-4}
3	0.8×10^{-2}	1.0×10^{-2}

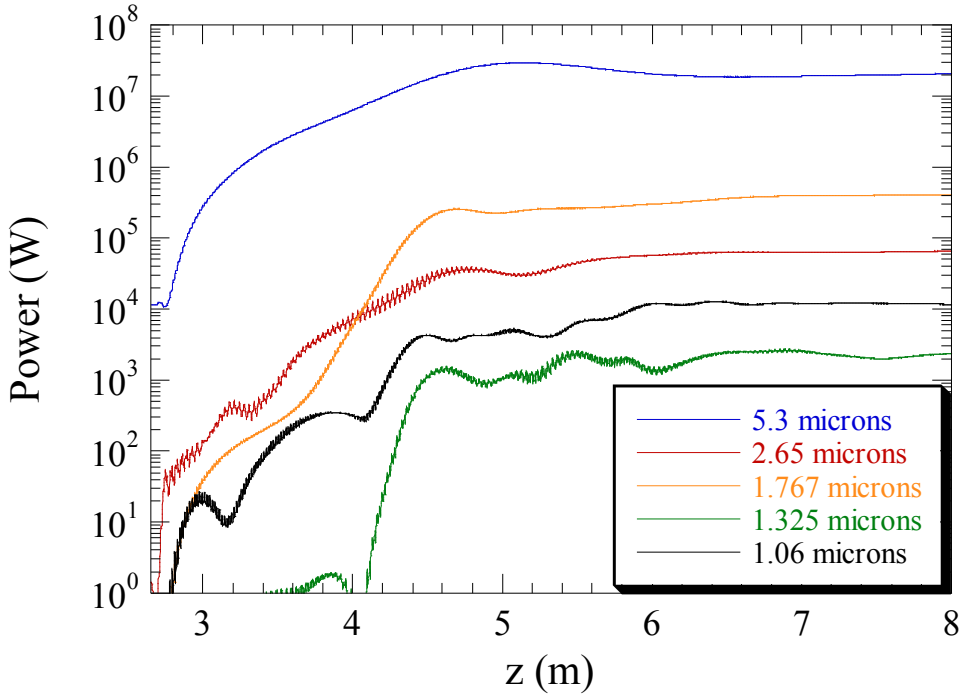

The SVEA approximation as implemented in MEDUSA is adequate even when the fields grow as rapidly as shown here.

OSCILLATOR SIMULATIONS WITH OPC

We have begun testing MEDUSA/ OPC integration for the JLab 10-kW Upgrade oscillator.

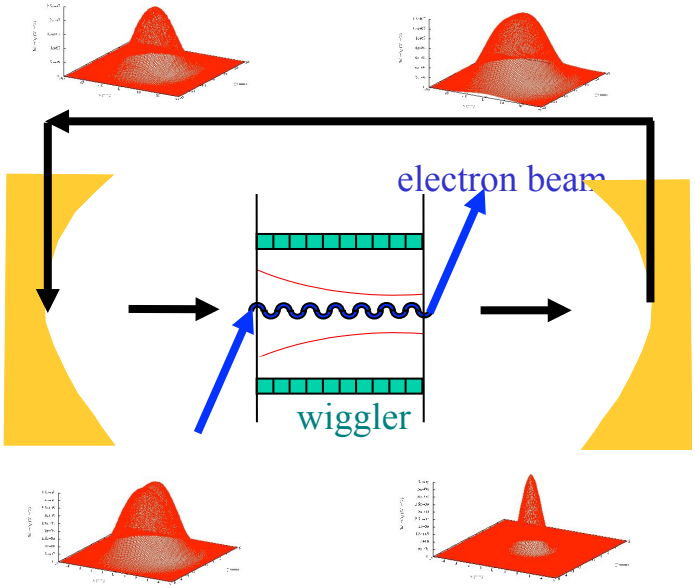

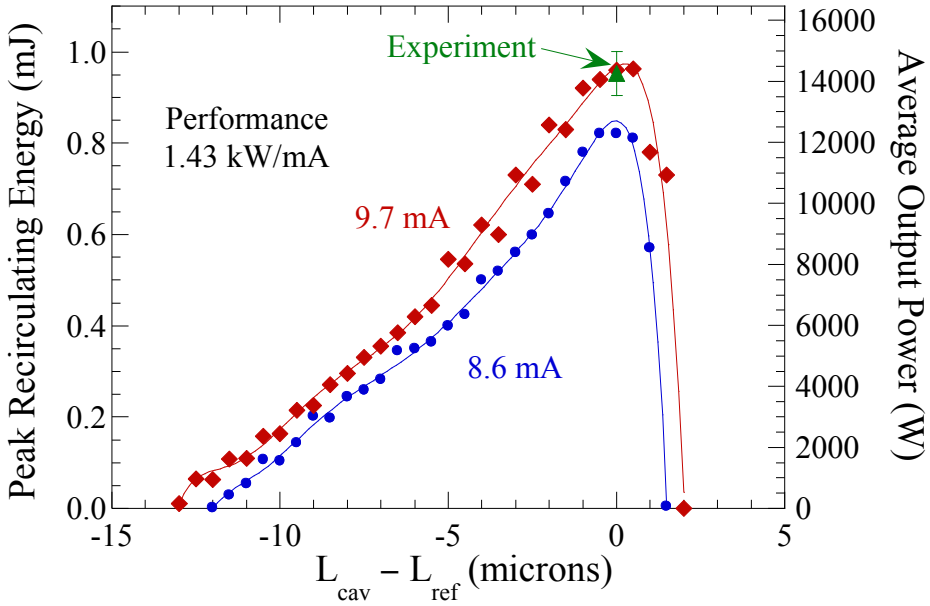

Comparison with the JLab experiment shows reasonable agreement. The best estimate of the average current is 8.6 mA, and the result is within 9% of the observed power.

OUTPUT POWER AND PULSE SHAPE

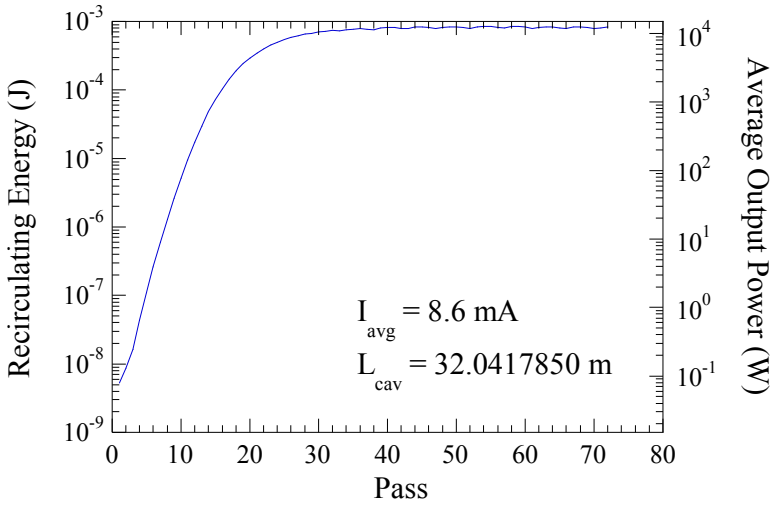

- The average output power in steady-state is about 12.3 kW for an average current of 8.6 mA
- JLab reports 14.26 (± 5%) kW
  - 13.5 – 15.0 kW
- Simulation is within about 9% of the experiment

- The output pulse shape is distorted due to slippage
  - Gradual rise in the tail and a shape drop at the head
- Peak pulse powers in the range of 4 - 5 GW

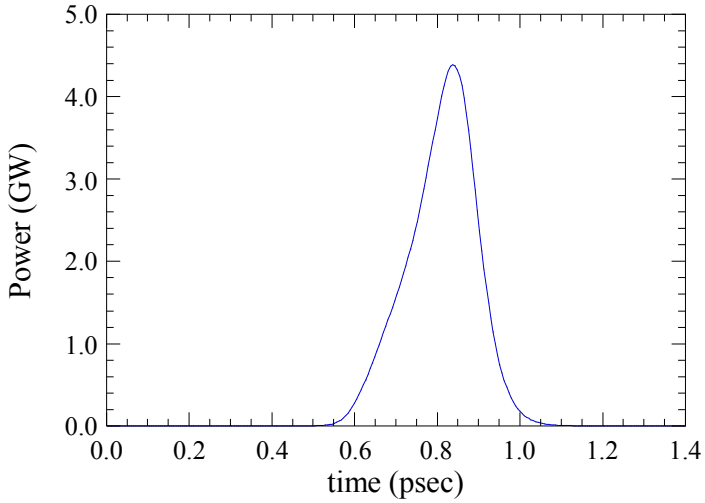

ELECTROMAGNETIC MODE PATTERNS

- Once the steady-state is reached, the mode quality is quite good
  - Mode patterns at right correspond to the **peak of the output pulse** and the **optimal cavity length**
  - As yet no attempt to determine M^2
- The mode at the wiggler exit displays little evidence of higher order modes
- Substantial expansion as the mode propagates to the downstream mirror
  - Transmissive out-coupling
- OPC can propagate the mode beyond the resonator

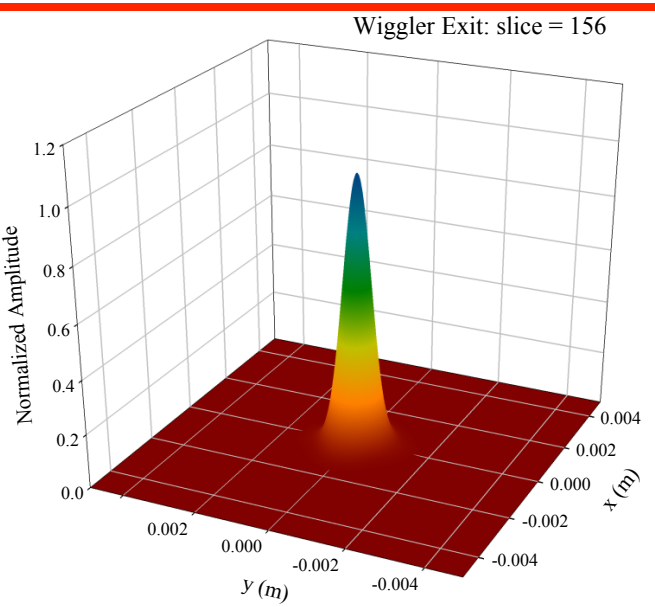

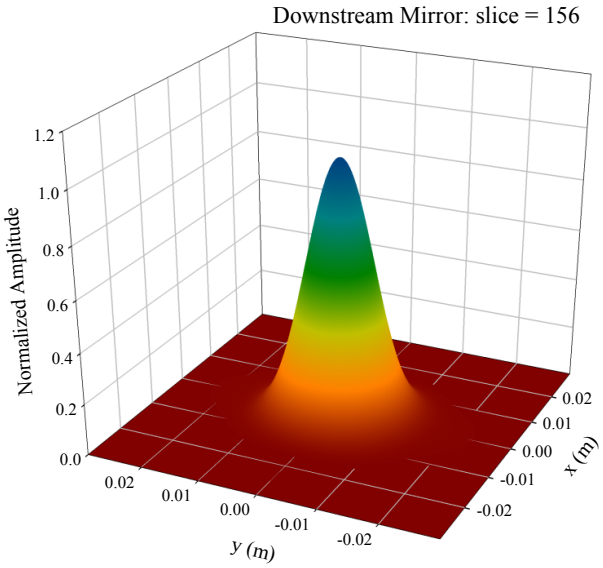

MODE SIZE ON THE MIRRORS

- OPC saves the evolution of the **rms** mode sizes on the upstream and downstream mirrors
- The downstream mirror is the output (transmissive) mirror
- Oscillations due to optical guiding in the wiggler that distorts the mode

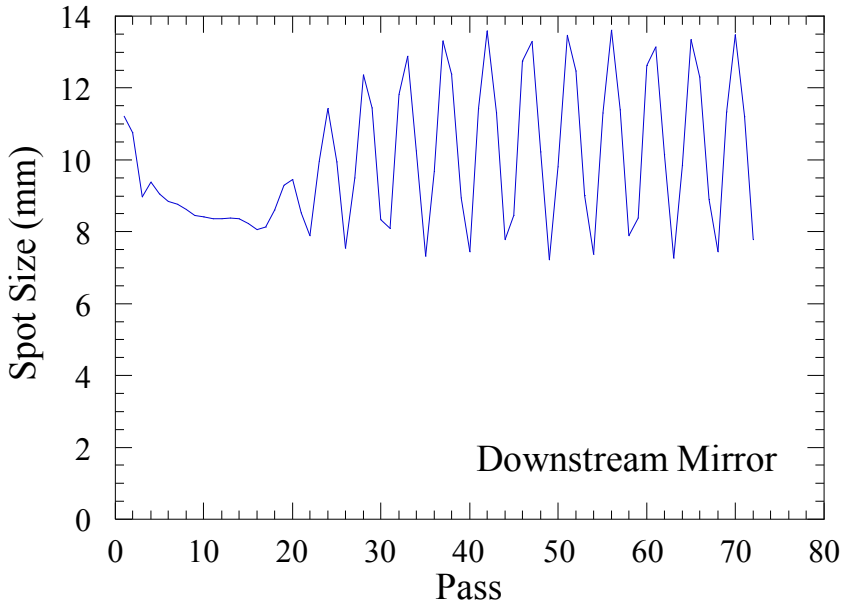

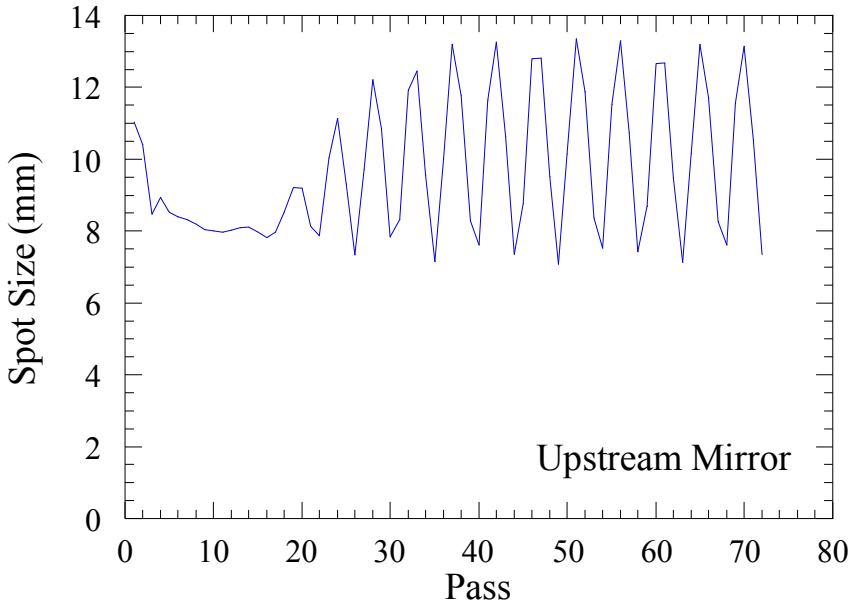

- Average rms mode size on each mirror is about 10-11 mm in the steady-state regime
- This is in good agreement with the observations at Jefferson Laboratory

DETUNING EXPERIMENT AT BNL

- It is well-known that detuning the beam energy off resonance can increase the extraction efficiency
- Experiment to demonstrate this was conducted at the BNL/SDL

APPLIED PHYSICS LETTERS **91**, 181115 (2007)

Efficiency enhancement using electron energy detuning in a laser seeded free electron laser amplifier

X. J. Wang,[a] T. Watanabe, Y. Shen, R. K. Li, J. B. Murphy, and T. Tsang
National Synchrotron Light Source, Brookhaven National Laboratory, Upton, New York 11973, USA

H. P. Freund
Science Applications International Corporation, McLean, Virginia 22102, USA

(Received 31 August 2007; accepted 9 October 2007; published online 31 October 2007)

We report the experimental characterization of efficiency enhancement in a single-pass seeded free-electron laser (FEL) where the electron energy is detuned from resonance. Experiments show a doubling of the efficiency for beam energies above the resonant energy. Measurements of the FEL spectra versus energy detuning shows that the wavelength is governed by the seed laser. The variation in the gain length with beam energy was also observed. Good agreement is found between the experiment and numerical simulations using the MEDUSA simulation code. © *2007 American Institute of Physics*. [DOI: 10.1063/1.2803772]

Energy	98-102 MeV
Bunch Charge	350 pC
Bunch Duration	1-2 psec
Normalized Emittance	4 mm-mrad
Energy Spread	0.1%
Wiggler Period	3.89 cm
Wiggler Length	10 m
Wiggler Amplitude	3 kG
Seed Wavelength	793.5 nm
Seed Power	4 kW
Seed Duration	6 psec

ENERGY DETUNING – OUPUT COMPARISONS

Comparison with experimental results on-resonance (100.86 MeV kinetic energy) shows good agreement

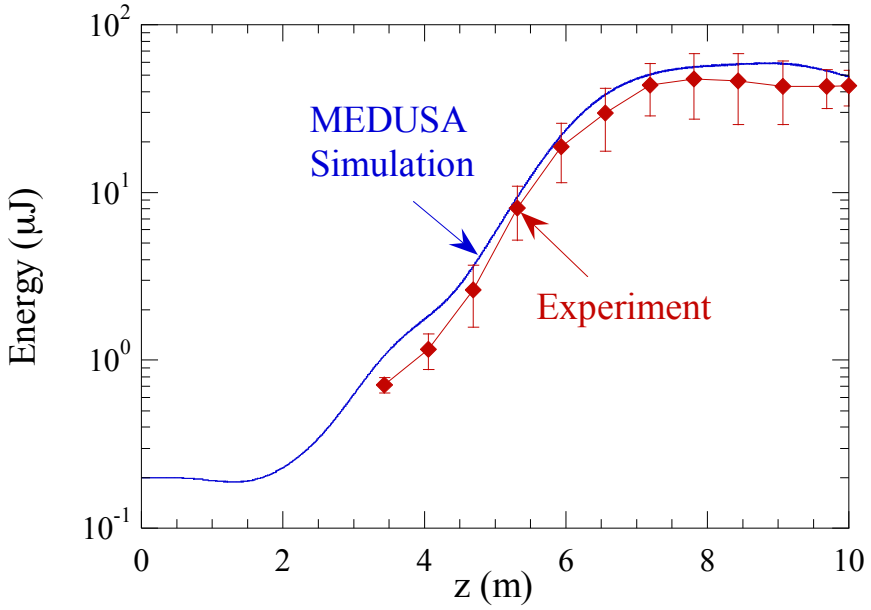

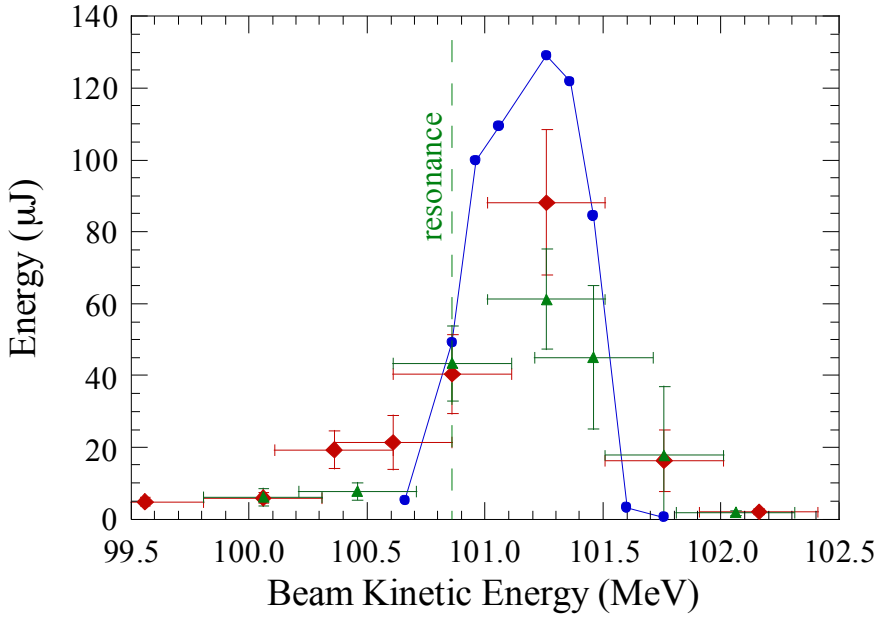

As the energy is detuned, experiment and simulation show expected increases in efficiency, with good agreement between simulation & experiment

ENERGY DETUNING - SPECTRA

- The spectra found in the experiment and in simulation for both the resonant and detuned beam energies are in good agreement

Off-Resonance

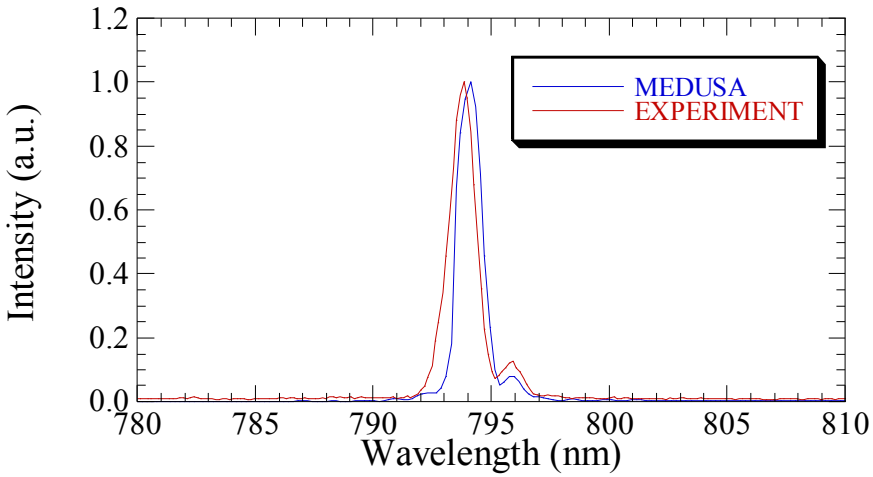

On-Resonance

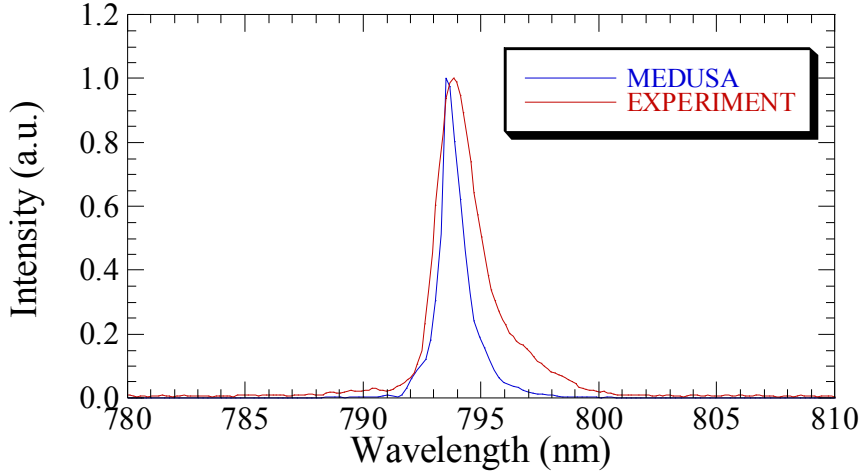

- The central wavelength is predominantly controlled by the seed laser wavelength

PROSPECTS FOR START-TO-END SIMULATIONS

- In development for x-ray SASE FEL Projects
- Multiple codes to handle beam production, transport, and FEL
  - PARMELA, ELEGANT, ASTRA, TRAFFIC4, etc.
    - not first principles models
  - NPS Codes, MEDUSA, FELIX, GINGER, GENESIS
    - 3-D FEL Codes are well-in-hand
    - some modifications may be needed to address specific physics
      - harmonics, real beam distributions, etc.
- **Purpose: Engineering Design Support**
- **Precursor to Engagement Model**
  - Atmospheric Propagation: High Energy Laser Code for Atmospheric Propagation (HELCAP)
    - NRL – 3-D, time-dependent, linear & nonlinear effects
  - Adaptive Optics, Lethality